NINJA: COSMOLOGICAL HYDRODYNAMICAL SIMULATIONS

R. SRIANAND@IUCAA

THE NISER-IUCAA NEW SIMULATIONS OF JWST GALAXIES AND QUASARS(NINJA)

- Galaxy evolution (including size evolution, metal enrichment history, standard relationships: BH mass vs Stellar Mass, Galactic Main-sequence, Mass-metallicity relations) and role played by the feedback.

- SMBH evolution and its contribution to the ionising and GW background. Understanding the "little red dots". The main issue is volume vs resolution.

- IGM and CGM evolution: How they are linked to the feedback process in galaxies.

- Cosmic reionization: Understanding the epoch of reionisation and effect on galaxy and BH growth.

- Galaxy merger history and large scale clustering.

THE NISER-IUCAA NEW SIMULATIONS OF JWST GALAXIES AND QUASARS(NINJA)

Run ID	CPU hrs ($\times 10^5$)	Model variation wrt fiducial	Final Redshift (z_f)	Storage Requested (Tb)	Status
Simulations run using PEGASUS					
NINJA_L50N2040f	6.0	None	4	60	completed
NINJA_L150N2040f	6.0	None	4	60	completed
NINJA_L250N2040f	4.0	None	5	51	completed
NINJA_L250N2040f1	5.0	fast wind	5	51	[redacted] Completed
NINJA_L150N2040v1	5.0	week wind	5	51	completed
NINJA_L150N2040v2	5.0	very weak wind	5	51	completed
NINJA_L150N2040v3	5.0	high BH seed	5	51	Planned
NINJA_L100N2500vh	5.0	higher resolution	7	51	Planned
Post-processing	4.0	UVB Fluctuations	5	40	Planned
Post-processing	3.0	Light synthesis	..	..	Planned
TOTAL (requested)	22	....	....	193	
Simulations run at NISER					
NINJA_L50N560f_n	5.0	None	5	51	completed
NINJA_L50N1008f_n	5.0	None	5	51	completed
NINJA_L50N1008f_nv1	5.0	slow wind	5	51	completed
NINJA_L50N1008f_nv2	5.0	very slow wind	5	51	completed
NINJA_L150N1008f_n	5.0	None	5	51	scheduled

Table 1: Details of NINJA runs and requirements for proposed runs. The runs (column 1) are labeled NINJA_LXXXY with XXX representing the boxsize in Mpc/h and Y taking a character value (f for fiducial and v for variation with respect to fiducial) which may be followed by a number to distinguish them from each other. The (_n) included shows the runs done at NISER. Column 2 is the actual CPU hours required, based on our runs in the previous cycle. The other columns are model variation with respect to fiducial, the final redshift proposed, the storage requirements of the proposed runs.

- Anirban Chakraborty
- Prakash Gaikwad + Manish Singh Almia
- Soumak Maitra + Suprio Saha
- Tirth + Vikram Khaire

ILLUSTRIS-TNG VS NINJA COMPARISON

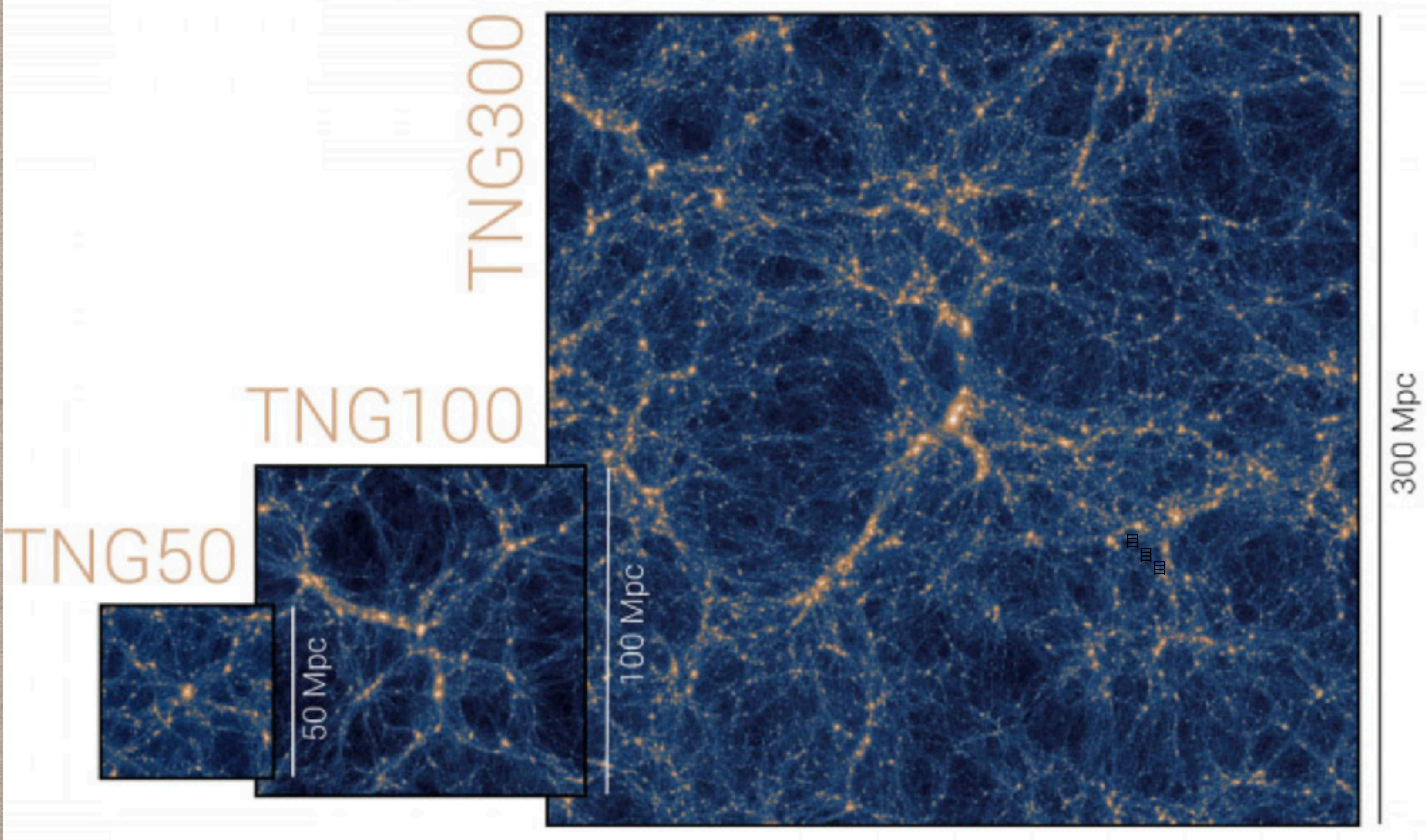

		TNG50	TNG100	TNG300
Volume	[Mpc^3]	51.7^3	110.7^3	302.6^3
L_{box}	[Mpc/h]	35	75	205
N_{GAS}	-	2160^3	1820^3	2500^3
N_{DM}	-	2160^3	1820^3	2500^3
N_{TR}	-	2160^3	2×1820^3	2500^3
m_{baryon}	[$\mathrm{M}_\odot$]	8.5×10^4	1.4×10^6	1.1×10^7
m_{DM}	[$\mathrm{M}_\odot$]	4.5×10^5	7.5×10^6	5.9×10^7
$\epsilon_{\mathrm{gas,min}}$	[pc]	74	185	370
$\epsilon_{\mathrm{DM},\star}$	[pc]	288	740	1480

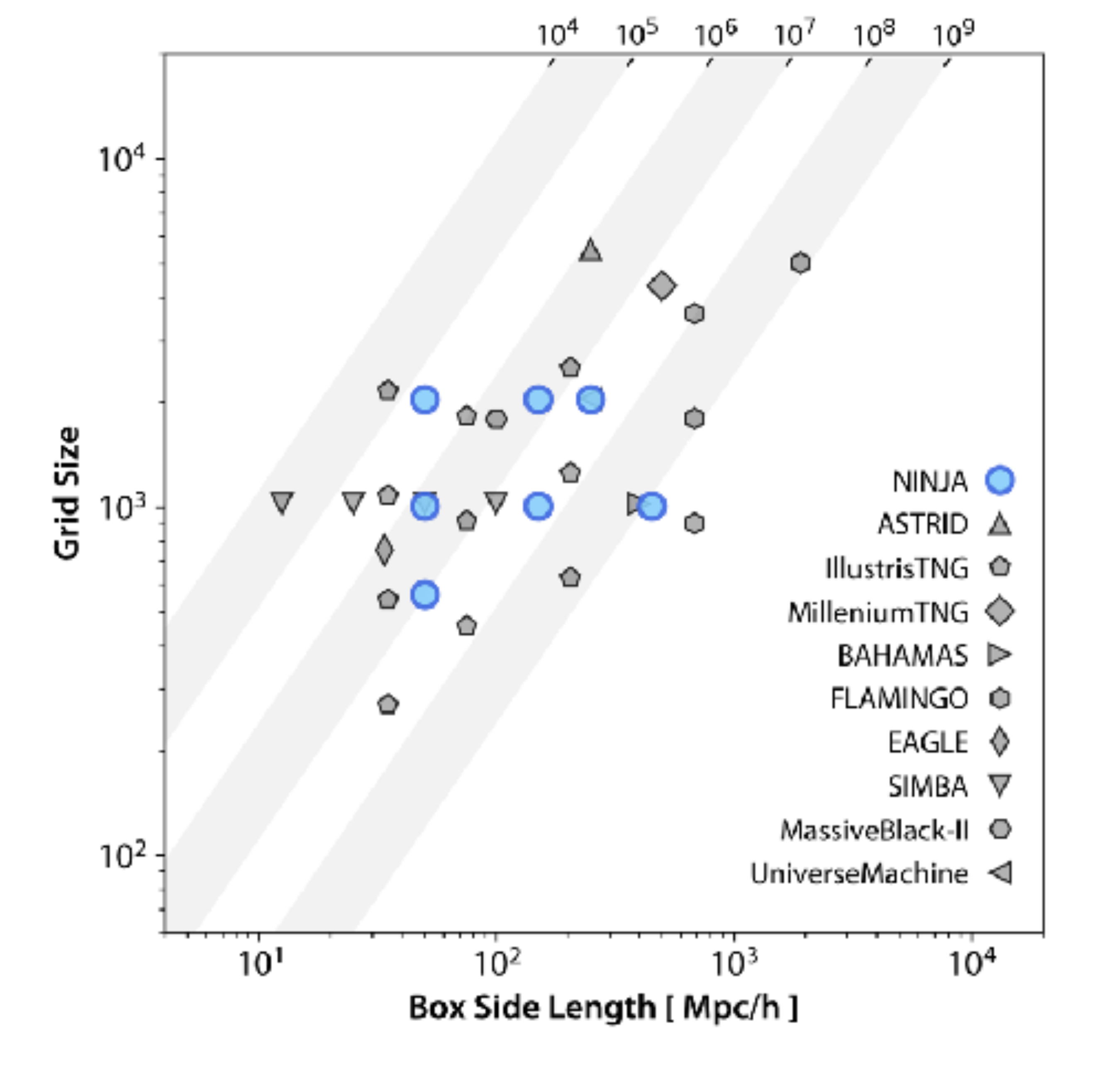

Table 1. Details of NINJA simulation boxes used in this study

Name	Values used in			Notes
	L50N2040	L150N2040	L250N2040	
$\mathrm{L_{Box}}$	50	150	250	Simulation box size in h^{-1} cMpc
$\mathrm{N_{DM}}$	2040^3	2040^3	2040^3	Number of dark matter particles
$\mathrm{N_{gas}}$	2040^3	2040^3	2040^3	Initial number of gas particles
$\mathrm{M_{DM}}$	1.09×10^6	2.93×10^7	1.36×10^8	Mass of a dark matter particle in $h^{-1}M_\odot$
$\mathrm{M_{gas}}$	2.01×10^5	5.44×10^6	2.52×10^7	Initial mass of a gas particle in $h^{-1}M_\odot$
z_{in}	189	99	99	Initial redshift
z_{fi}	5	5	5	Final redshift
ϵ_{grav}	0.82	2.45	4.08	Gravitational softening length in h^{-1}kpc
Seed	140425	150478	121024	Seed used to generate Initial Conditions

RADIATION FIELD AND SELF-SHIELDING:

- Option 1: Uniform background with <x(HI)> is the filling factor.
- Option 2: Two phase (ionised regions + neutral islands)
- Option 3: Hybrid model with post-processing for deionisation at each step.
- Option 4: Full radiative transport.

EXAMPLE OF TREECOOL FILE

# log(1+z)	g_HI	g_HeI	g_HeII	q_HI	q_HeI	q_HeII
0E+00	1.02E-13	4.5E-14	1.2E-15	6.5E-26	2.1E-26	5.4E-28
1E-01	1.15E-13	5.1E-14	1.45E-15	7.2E-26	2.4E-26	6.8E-28
...						
1E+00	9.5E-12	4.2E-12	1.1E-13	5.8E-24	1.9E-24	4.2E-26

STAR FORMATION: (Springel & Hernquist, 2003, MNRAS, 339, 289)

Density evolution

$$\frac{\mathrm{d}\rho_c}{\mathrm{d}t} = -\frac{\rho_c}{t_\star} - A\beta\frac{\rho_c}{t_\star} + \frac{1-f}{u_h - u_c}\Lambda_{net}(\rho_h, u_h),$$

$$\frac{\mathrm{d}\rho_h}{\mathrm{d}t} = \beta\frac{\rho_c}{t_\star} + A\beta\frac{\rho_c}{t_\star} - \frac{1-f}{u_h - u_c}\Lambda_{net}(\rho_h, u_h).$$

Energy evolution

$$\frac{\mathrm{d}}{\mathrm{d}t}(\rho_c u_c) = -\frac{\rho_c}{t_\star}u_c - A\beta\frac{\rho_c}{t_\star}u_c + \frac{(1-f)u_c}{u_h - u_c}\Lambda_{net},$$

$$\frac{\mathrm{d}}{\mathrm{d}t}(\rho_h u_h) = \beta\frac{\rho_c}{t_\star}(u_{SN} + u_c) + A\beta\frac{\rho_c}{t_\star}u_c - \frac{u_h - f u_c}{u_h - u_c}\Lambda_{net}.$$

$$A(\rho) = A_0\left(\frac{\rho}{\rho_{th}}\right)^{-4/5},$$

$$t_\star(\rho) = t_0^\star\left(\frac{\rho}{\rho_{th}}\right)^{-1/2},$$

STAR FORMATION

$\rho_{\star c}$	57.7	Critical over density
β	0.1	Fraction of the gas energy which is locally returned as supernovae on star formation
T_C	10^3	Temperature of the cold star forming clouds in K
T_{SN}	10^8	Temperature of the supernova remnants in K
A_0	1000	Parameter of the SH03 model controlling the energy of the hot gas
$t_{\star 0}$	1.5	Maximum star formation time in units of density threshold
N_g	4	Number of star particle produces per gas particle

STAR FORMATION:

Observationally, there appears to be a tight correlation between disc-averaged measurements of the star formation rate per unit area and the gas surface density, a 'global Schmidt law', given by Kennicutt (1998) as

$$\Sigma_{\mathrm{SFR}} = (2.5 \pm 0.7) \times 10^{-4} \left(\frac{\Sigma_{\mathrm{gas}}}{\mathrm{M}_\odot\, \mathrm{pc}^{-2}} \right)^{1.4\pm0.15} \frac{\mathrm{M}_\odot}{\mathrm{yr\, kpc}^2}. \qquad (24)$$

$$t_{\mathrm{SFR}} = \frac{\Sigma_{\mathrm{gas}}}{\Sigma_{\mathrm{SFR}}} = 3.2\ \mathrm{Gyr} \left(\frac{\Sigma_{\mathrm{gas}}}{10\, \mathrm{M}_\odot\, \mathrm{pc}^{-2}} \right)^{-1/2}. \qquad (25)$$

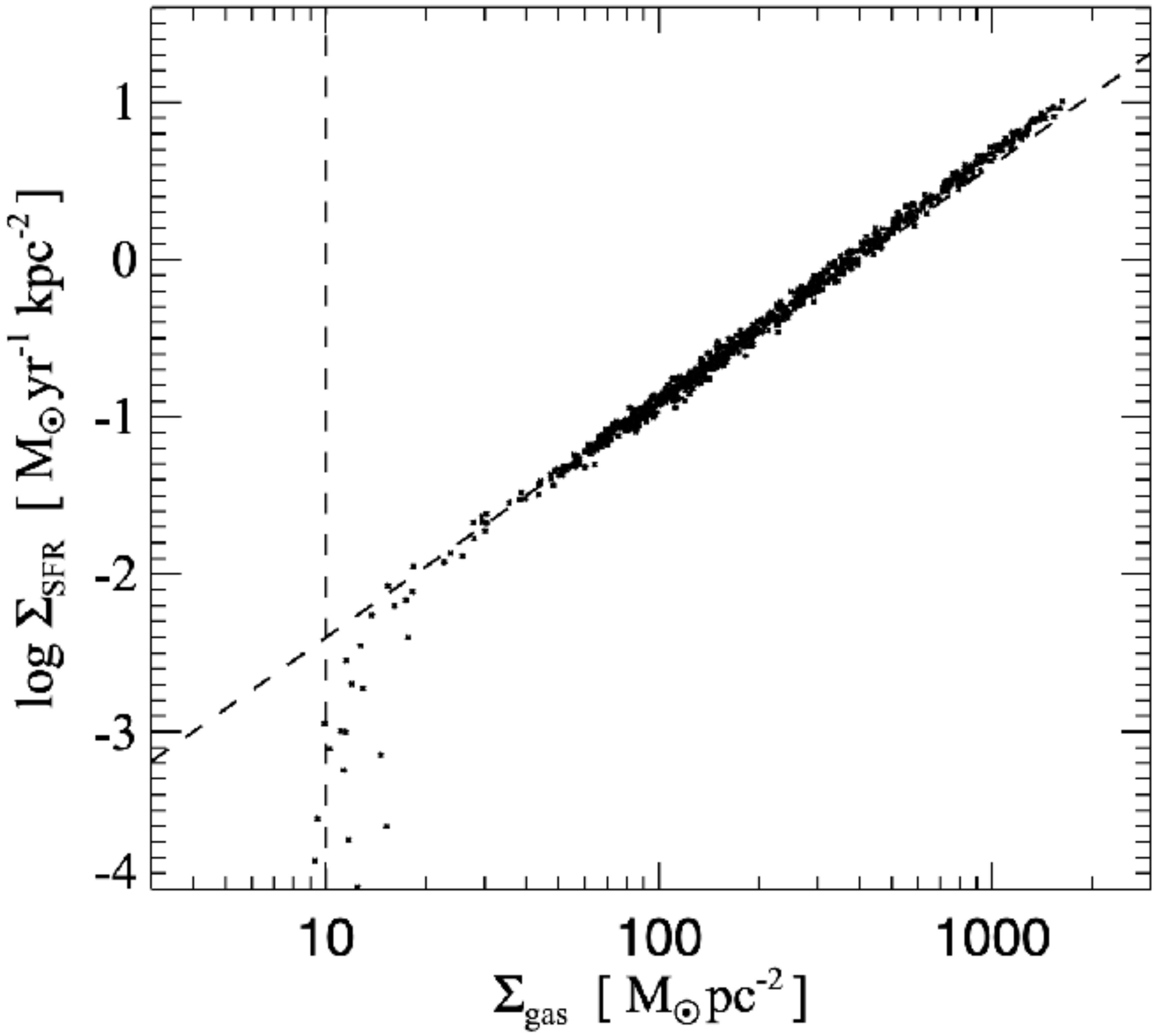

Figure 3. Star formation rate per unit area versus gas surface density in a self-consistent simulation of a disc galaxy that quiescently forms stars. The symbols show azimuthally averaged measurements obtained for our fiducial choice of $t_0^\star = 2.1$ Gyr. The dashed inclined line gives the Kennicutt law of equation (25), and the vertical line marks the observed cut-off of star formation.

STAR FORMATION: (Springel & Hernquist, 2003, MNRAS, 339, 289)

- Self regulated conditions - Energy input from the SNe explosions is equal to the gas cooling rate.
- Evolution of cold gas mass fraction (x).
- $\dot{M}_* = (1 - \beta)xm/t_*$
- $P_* = \frac{m}{m_*}\left\{1 - \frac{exp(1 - \beta)x\Delta t}{t_*}\right\}$ with $m_* = m_0/N_g$
- A new star particle is released when a random generated between 0 and 1 falls below P_*.

STAR FORMATION:

2.4. *Star formation*

Star are allowed to form in gas cells that have a thermal Jeans length smaller than the cell size,

$$L_J = \sqrt{\pi c_s^2 / G\rho} < \Delta x \,, \tag{9}$$

where c_s is the sound speed, G is Newton's gravitational constant, ρ is the density of the cell, and Δx is the cell radius which is calculated assuming spherical geometry. This ensures that the stars are only formed when the Jeans length becomes unresolved and the gravitational collapse can no longer be followed accurately (Truelove et al. 1997). This condition can allow for low-density gas outside the ISM of galaxies to form stars if it is relatively cold. To avoid this issue, we include an additional condition that the gas must be at least denser than $n_H = 10\ \mathrm{cm}^{-3}$ to be eligible to form stars. Gas cells that satisfy both criteria are converted to stars using the usual probabilistic approach (Springel & Hernquist 2003), which assumes that the star-formation rate is proportional to the gas density and inversely proportional to the local free fall time ($t_{ff} = \sqrt{3\pi/32G\rho}$)

$$\mathrm{SFR} = \epsilon_{ff}\, \rho / t_{ff} \,, \tag{10}$$

where ϵ_{ff} is the star formation efficiency per free-fall time of gas. In our simulations, we set this efficiency to 100% to prevent the unresolved gas from artificially collapsing to high densities (Hu et al. 2023). We have performed simulations with other values of ϵ_{ff}, varying it all the way from 1 – 100%. This parameter does not have any significant effect on the global properties of the simulated galaxies, which is in agreement with previous works that investigated the impact of ϵ_{ff} in

SUPERNOVAE WINDS AND STELLAR FEEDBACK

(Okamoto et al 2010; Vogelsberger et al. 2013)

[redacted] Therefore, the mass flux in the winds in the 'vw' models, $\dot{M}_{\rm w}$, can be written as

$$\dot{M}_{\rm w} = 2\frac{\dot{E}_{\rm SN}}{v_{\rm w}^2} \propto \frac{\dot{M}_*}{\sigma^2}, \qquad \text{with } v_w = \kappa_w \sigma \tag{6}$$

because the wind speed, $v_{\rm w}$, is proportional to the local dark matter velocity dispersion, σ. From these considerations, the wind mass-loading, $\eta_{\rm w}$, can be expressed as

$$\eta_{\rm w} \equiv \frac{\dot{M}_{\rm w}}{\dot{M}_*} = \left(\frac{\sigma}{\sigma_0}\right)^{-2}, \tag{7}$$

where σ_0 is a parameter defined by the IMF and the feedback efficiency. [redacted]

- Velocity dispersion is calculated locally. This was shown to be proportional to halo velocity dispersion.
- Wind particles do not experience or produce pressure forces, nor may they be accreted on to the blackholes.
- They do receive mass return, cool and contribute to the density estimates.

STELLAR WIND FEEDBACK

σ_0	353 km/s	Square root of energy ejection rate. Controls mass loading
$\kappa_{\rm w}$	3.7	Wind speed to local particle velocity dispersion
$l_{\rm free}$	20	Wind free travel length in kpc/h
$t_{\rm free}$	60	Wind free travel time in Myr/h
$\rho_{\rm free}$	0.1	Wind free travel density factor in units of threshold density

$\sigma_0 = 353, 250, 185$ km/s

$\kappa_W = 3.7, 1.85, 7.4$

SUPERNOVAE WINDS AND STELLAR FEEDBACK

$$v_w = \max\left[\kappa_w\,\sigma_{\rm DM}\left(\frac{H_0}{H(z)}\right)^{1/3},\ v_{w,\rm min}\right],$$

environments. Taken together, the mass loading factor at injection is

$$\eta_w \equiv \frac{\dot{M}_w}{\dot{M}_{\rm SFR}} = \frac{2}{v_w^2}\, e_w(1-\tau_w), \qquad (2)$$

where $\dot{M}_w$ denotes the rate of gas mass to be converted into wind particles and $\dot{M}_{\rm SFR}$ the instantaneous, local star formation rate.

The wind energy available to a star-forming gas cell with metallicity Z is given by

$$e_w = \bar{e}_w\left[f_{w,Z} + \frac{1-f_{w,Z}}{1+(Z/Z_{w,\rm ref})^{\gamma_{w,Z}}}\right] \times N_{\rm SNII}\, E_{\rm SNII,51}\, 10^{51}\ {\rm erg}\ {\rm M}_\odot^{-1}, \qquad (3)$$

similar to the parametrization by Schaye et al. (2015).

METAL YIELDS:

$$\Delta M_i(t, \Delta t, Z) = \int_{\mathcal{M}(t+\Delta t)}^{\mathcal{M}(t)} (y_i + m\ Z_i\ f_{\rm rec}(m, Z))\ \Phi(m)\,\mathrm{d}m.$$

- $f_{rec}(m, Z)$ is the stellar recycling fraction is the total fraction of mass that is recycled into the ISM during the entire life-time of the star of mass m.
- Y_i is the yield (SNe for very massive stars + AGB for intermediate mass stars)
- H, He, C, N, O, Ne, Mg, Si and Fe are tracked. Total metallicity is also tracked separately.

BLACK HOLES:

BH sink particles grow in mass by accreting surrounding gas or through BH mergers. In our model, BH accretion is described using a Bondi–Hoyle–Lyttleton-based Eddington-limited rate

$$\dot{M}_{\rm BH} = \min\left[\frac{4\pi\alpha G^2 M_{\rm BH}^2 \rho}{(c_s^2 + v_{\rm BH}^2)^{3/2}}, \dot{M}_{\rm Edd}\right], \tag{21}$$

		BLACKHOLE SEEDING, ACCRETION
$M_{\rm HALO}^{(0)}$	$5 \times 10^9 M_\odot/h$	Minimum FOF halo mass to for seeding.
$M_{\rm STAR}^{(0)}$	$1 \times 10^7 M_\odot/h$	Minimum FOF stellar mass fo seeding
$M_{\rm BH,min}^{(0)}$	$3 \times 10^4 M_\odot/h$	Minimum seed blackhole mass
$M_{\rm BH,max}^{(0)}$	$3 \times 10^5 M_\odot/h$	Maximum seed bloackhole mass
$n_{\rm BH}^{(0)}$	-2	Seeding power law index.
$\alpha_{\rm acc}$	100	Accretion factor.
$\beta_{\rm edd}$	2	Eddington Factor.

BLACK HOLES: FEEDBACK

At high accretion state.

$$\Delta \dot{E}_{\rm high} = \epsilon_{\rm f,high} \epsilon_{\rm r} \dot{M}_{\rm BH}\, c^2,$$

At low accretion state (kinetic feedback)

$$\Delta \dot{E}_{\rm low} = \epsilon_{\rm f,kin} \dot{M}_{\rm BH} c^2.$$

$$\epsilon_{\rm f,kin} = \min\left(\frac{\rho}{f_{\rm thresh}\rho_{\rm SFthresh}}, 0.2\right)$$

BLACKHOLE FEEDBACK		
$\epsilon_{\rm TF}$	0.05	Blackhole feedback efficiency for thermal feedback.
$\chi^0_{\rm thr,max}$	0.1	Kinetic feedback Eddington threshold factor
χ_0	0.002	Kinetic feedback Eddington M factor for kinetic feedback
$M_{\rm pivot}$	0.01 = $10^8 M_\odot/h$	Kinetic feedback Eddington M pivot
$\beta_{\rm pivot}$	2	Kinetic feedback Eddington M index
$\epsilon_{\rm KF,max}$	0.2	Kinetic feedback
$\rho_{\rm thres}$	2	Kinetic feedback
$f_{\rm re}$	20	Kinetic feedback release factor

NINJA: GAS FLOW IN THE COSMIC TIME

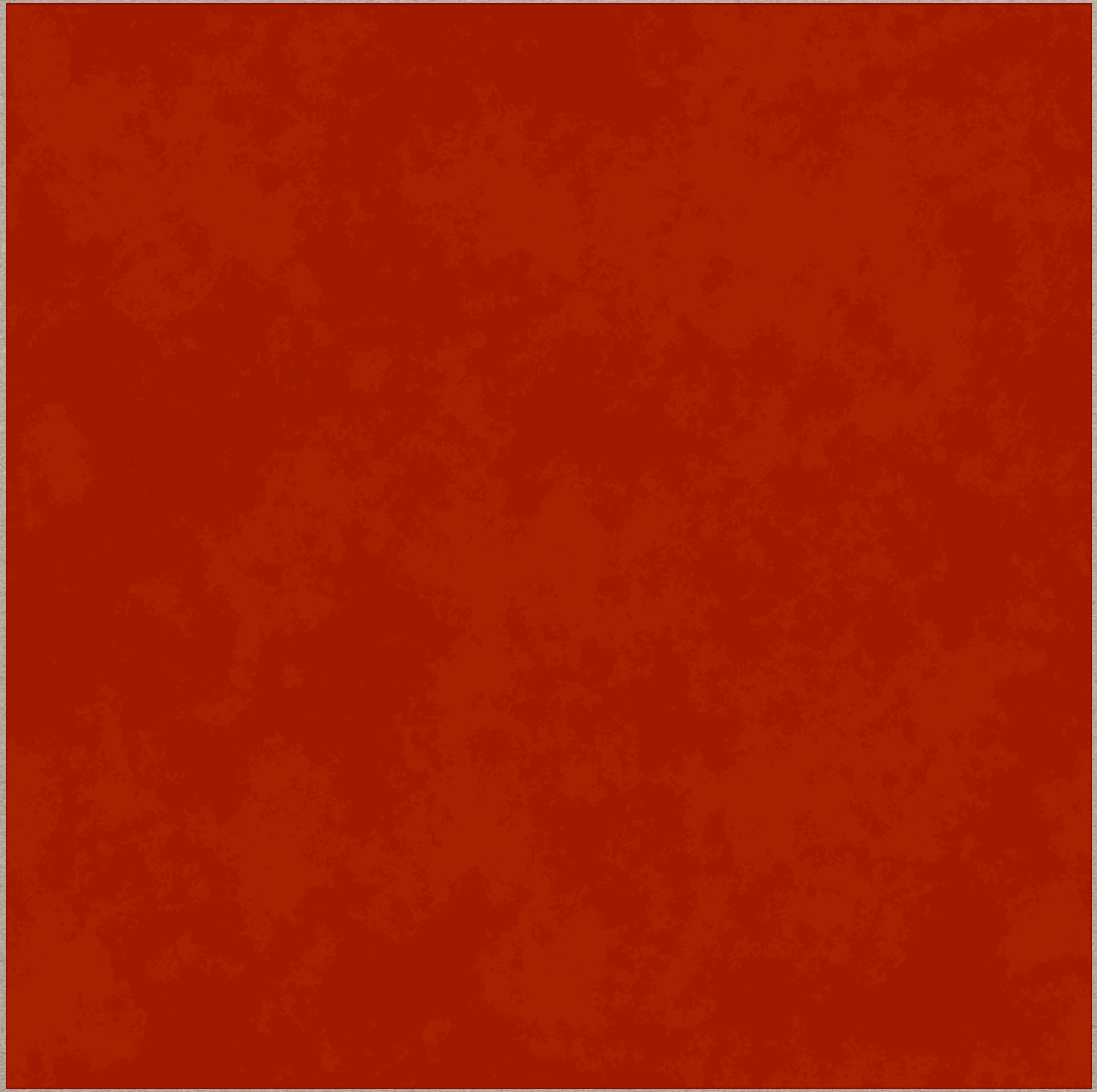

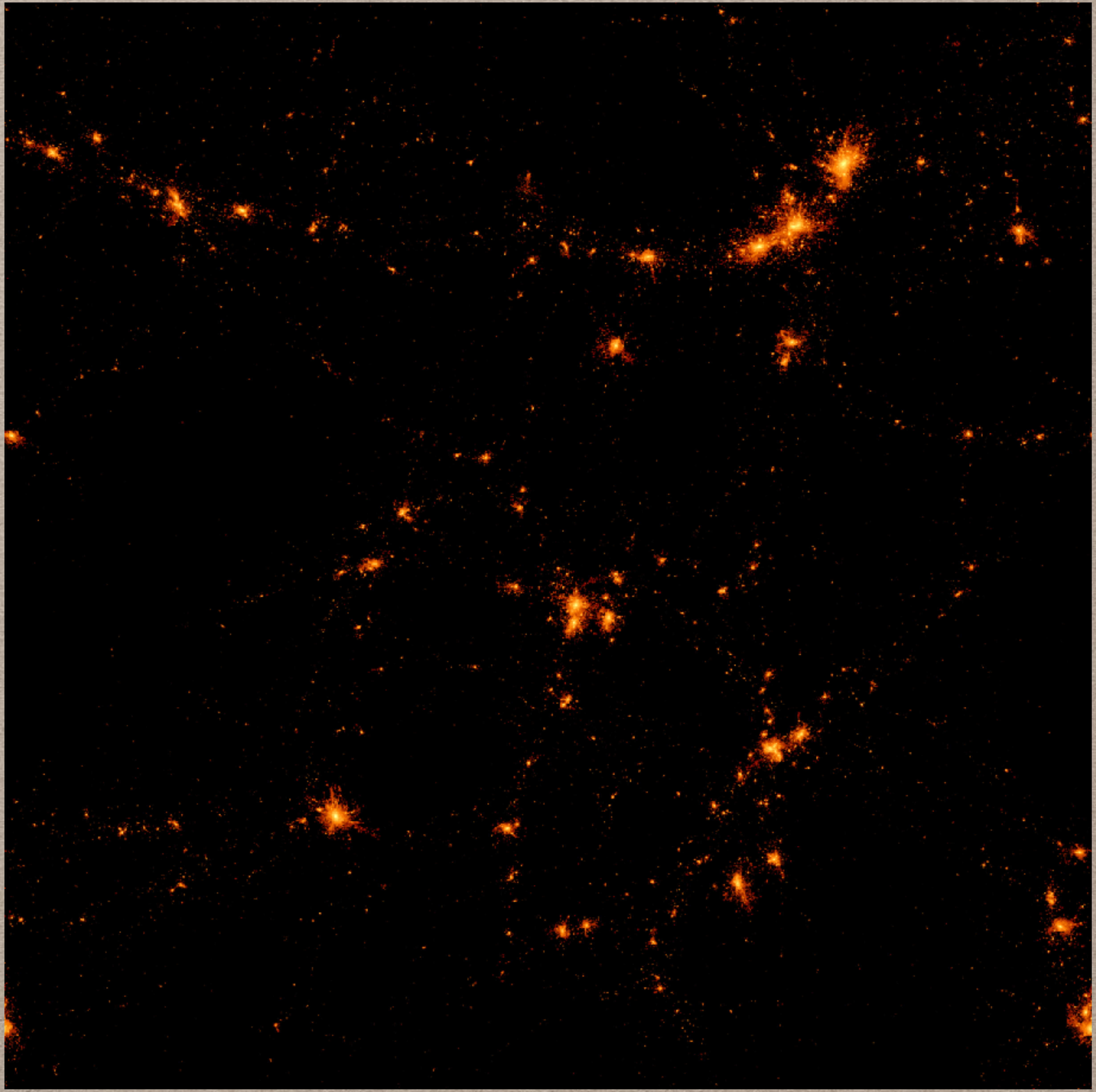

THE NISER-IUCAA NEW SIMULATIONS OF JWST GALAXIES AND QUASARS(NINJA)

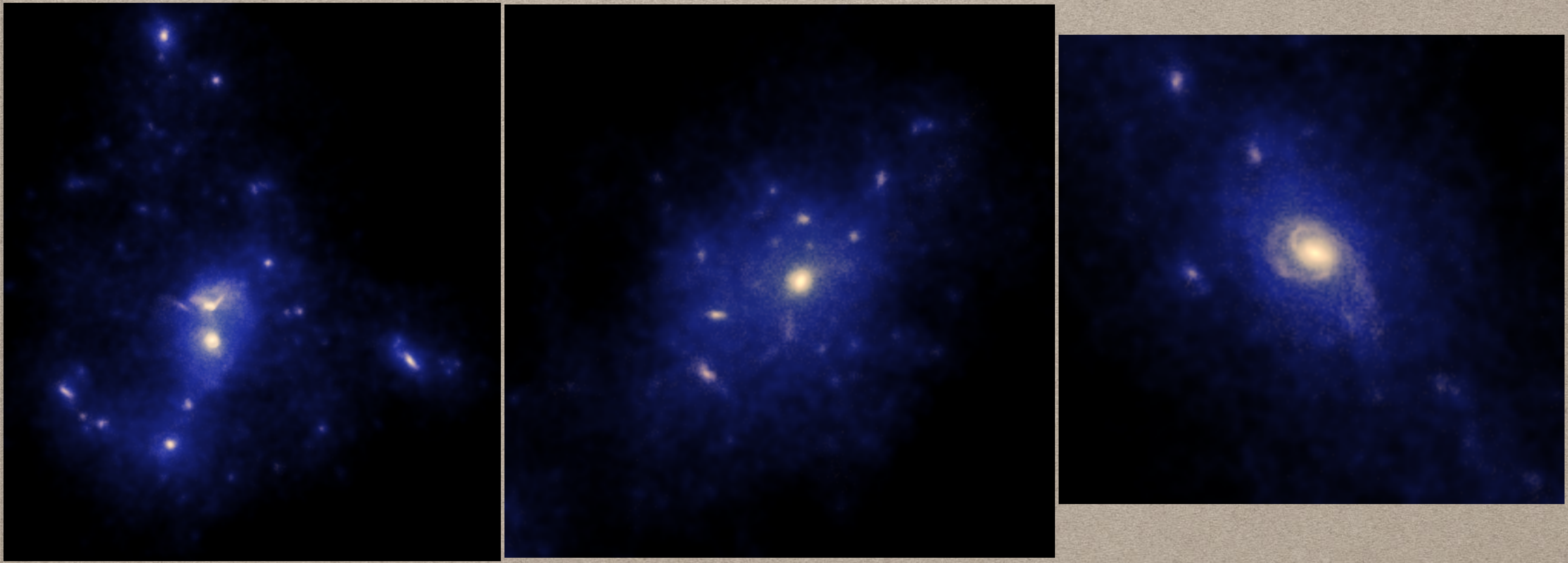

NINJA: MULTICOMPONENT DISTRIBUTION

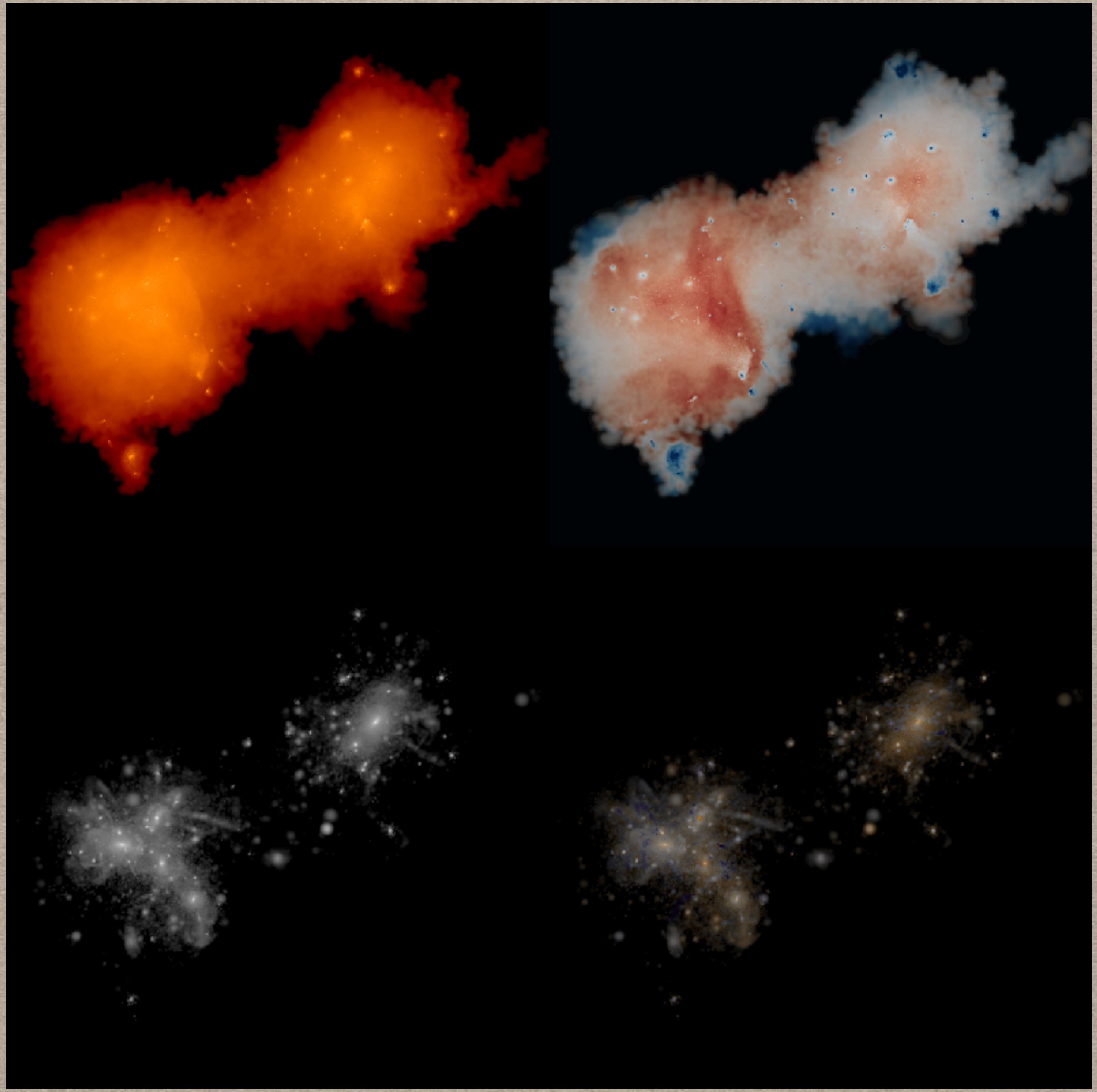

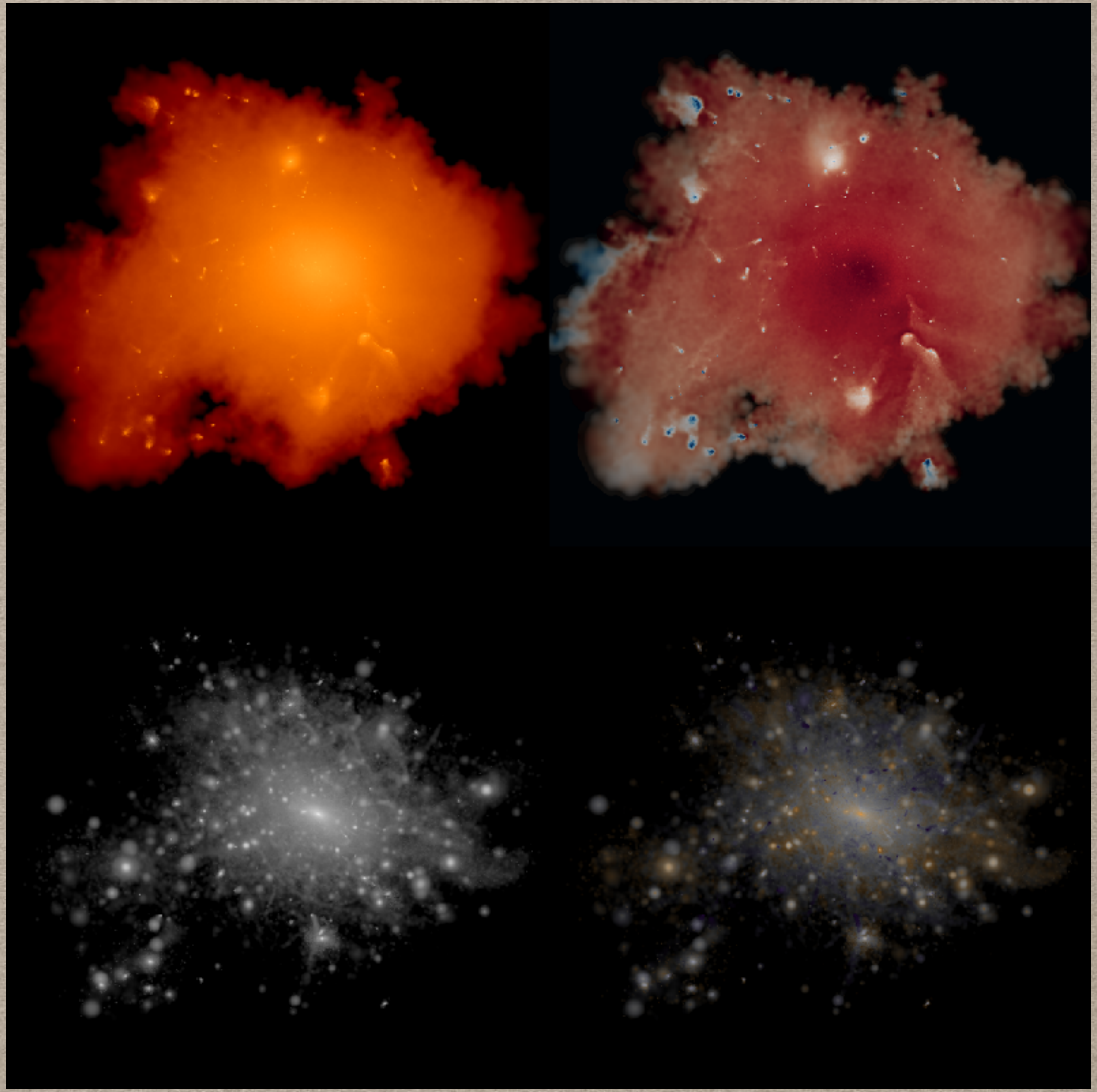

DM VS STELLAR MASS RELATIONSHIP & STELLAR MASS FUNCTION

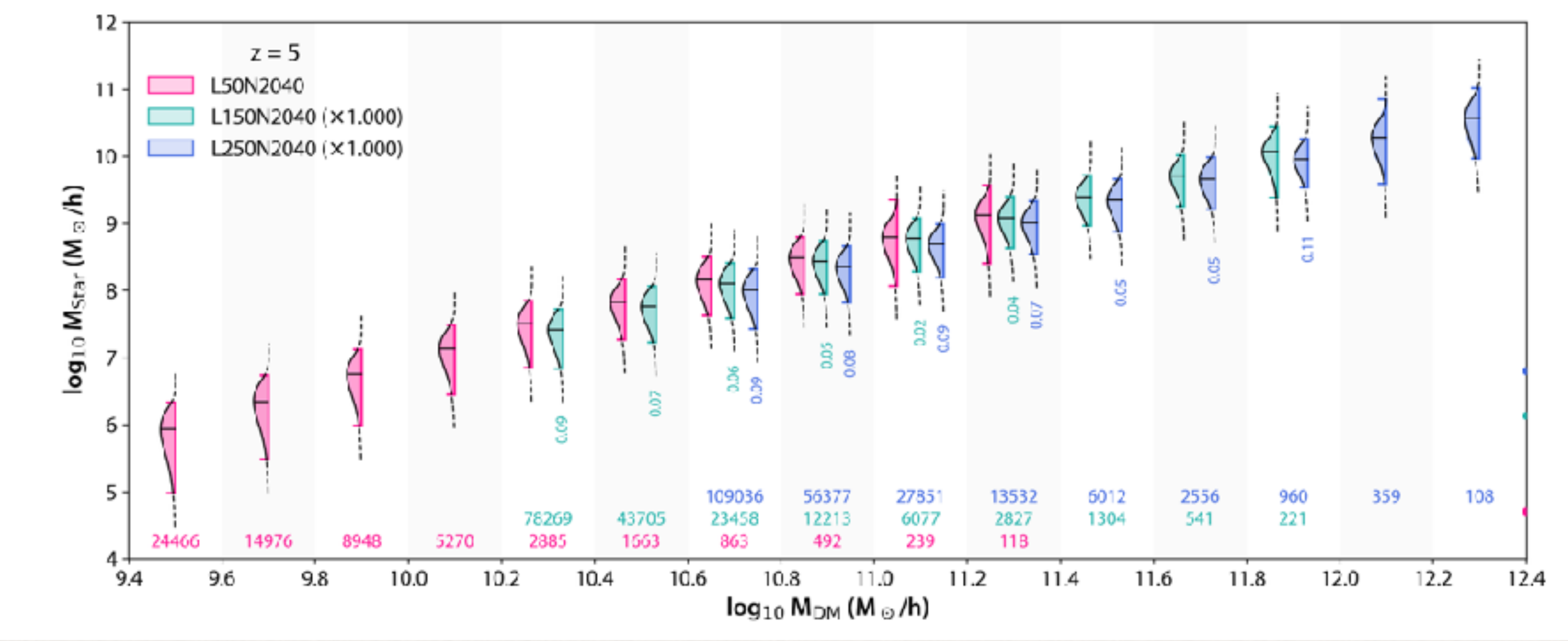

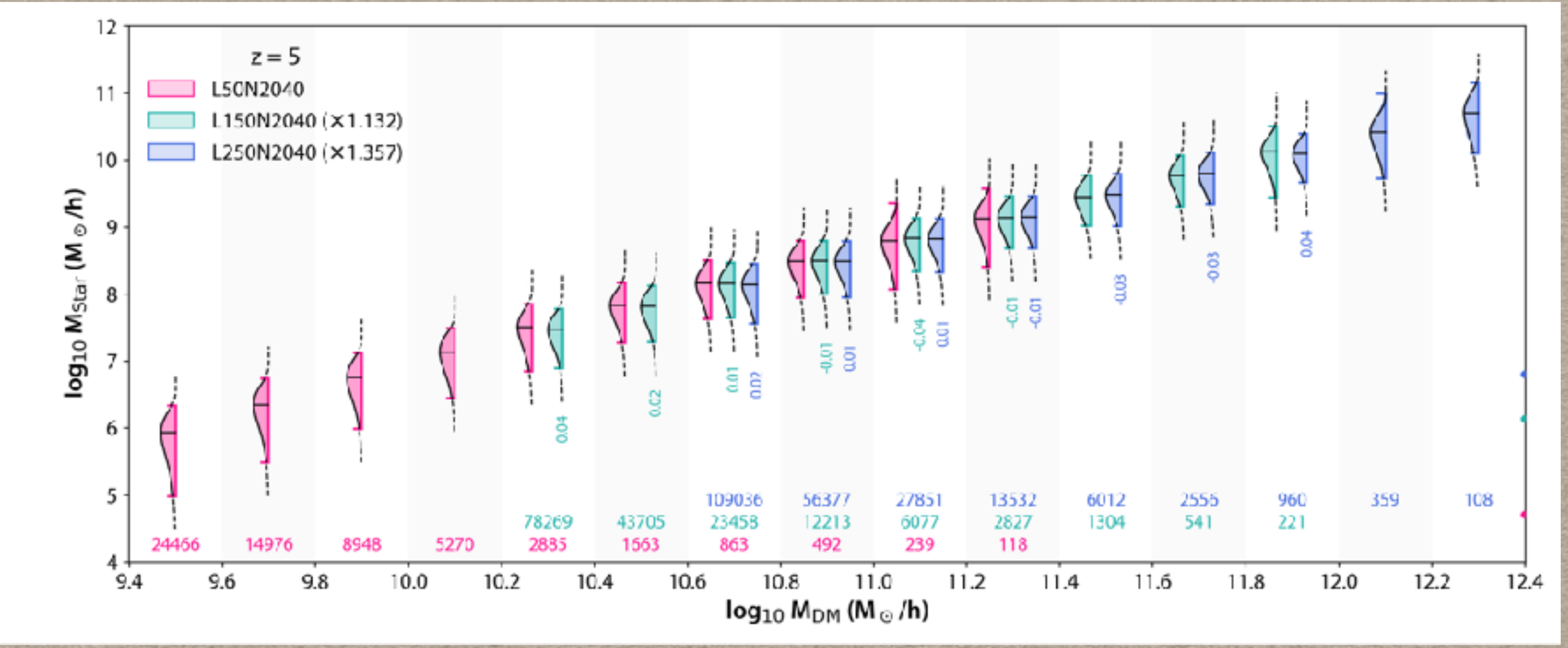

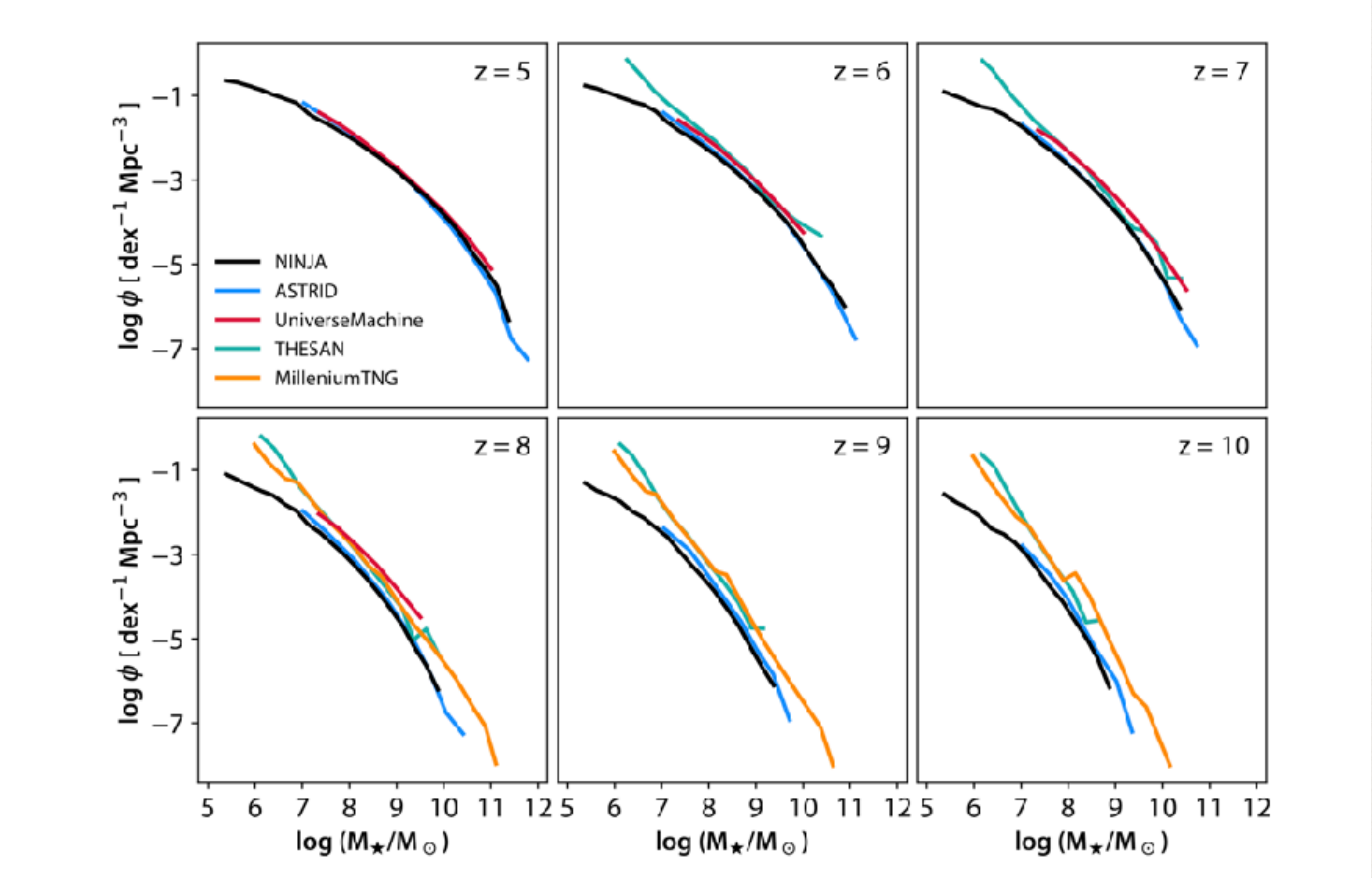

DM VS STELLAR MASS RELATIONSHIP & STELLAR MASS FUNCTION

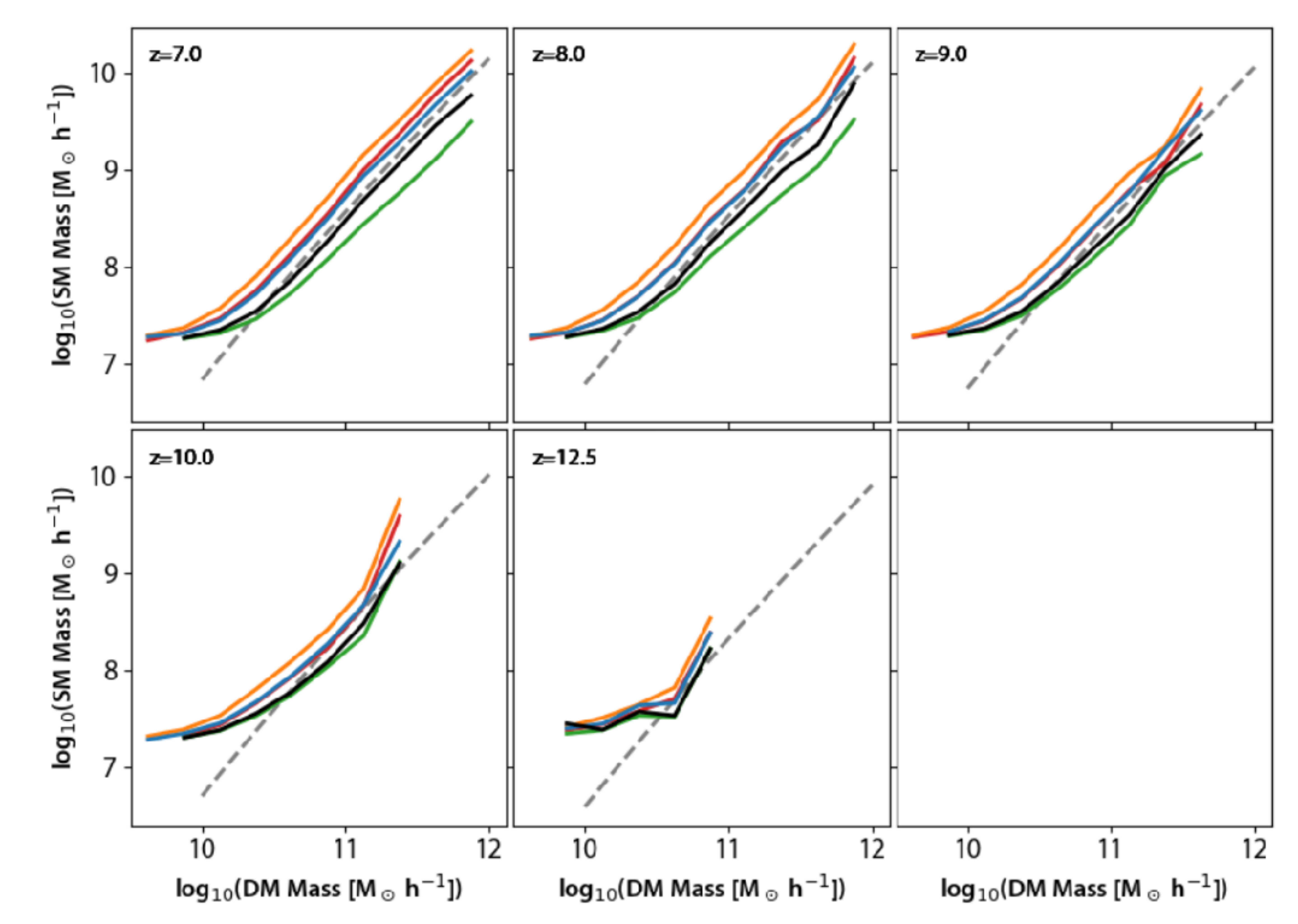

MORE RELATIONS!

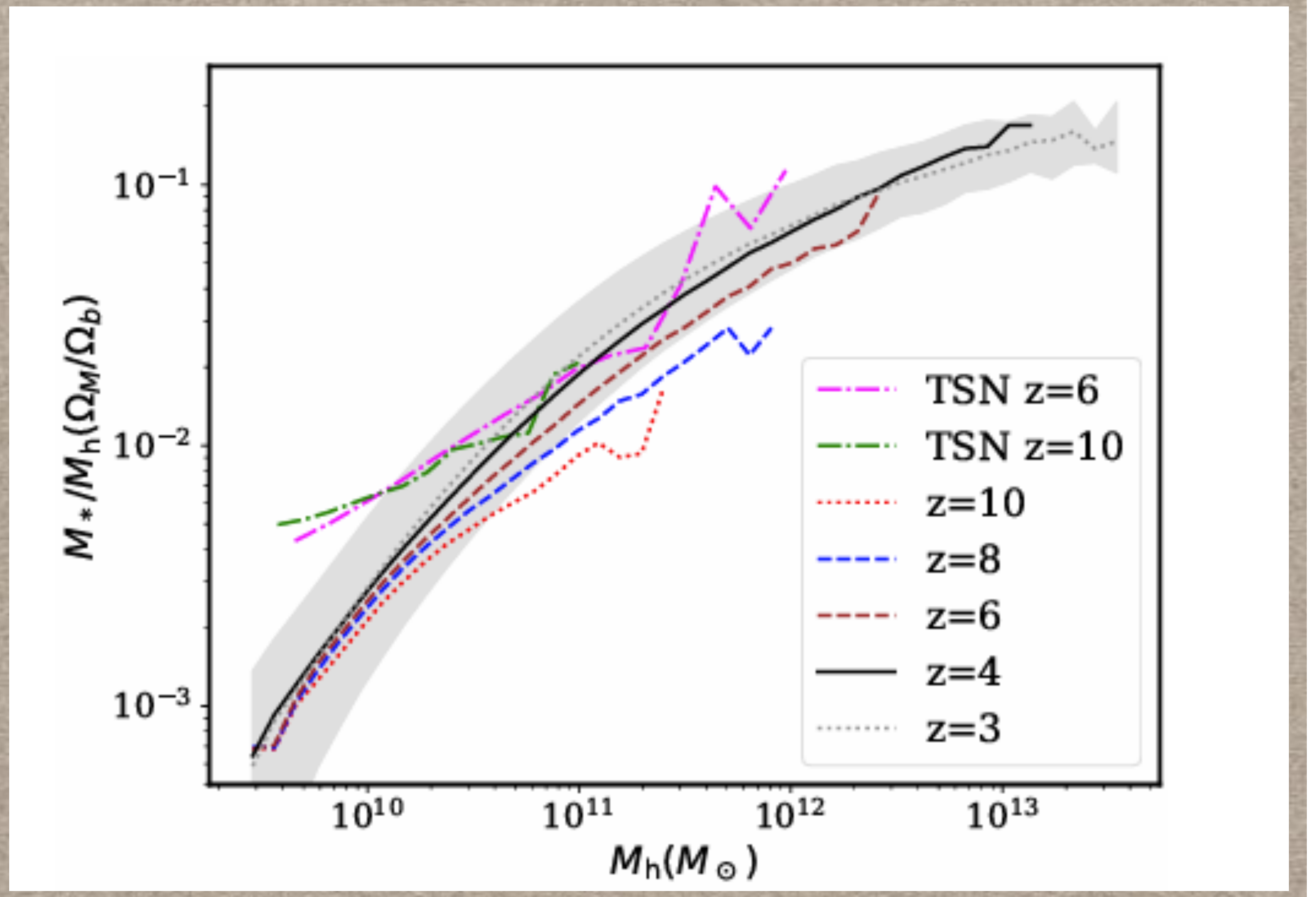

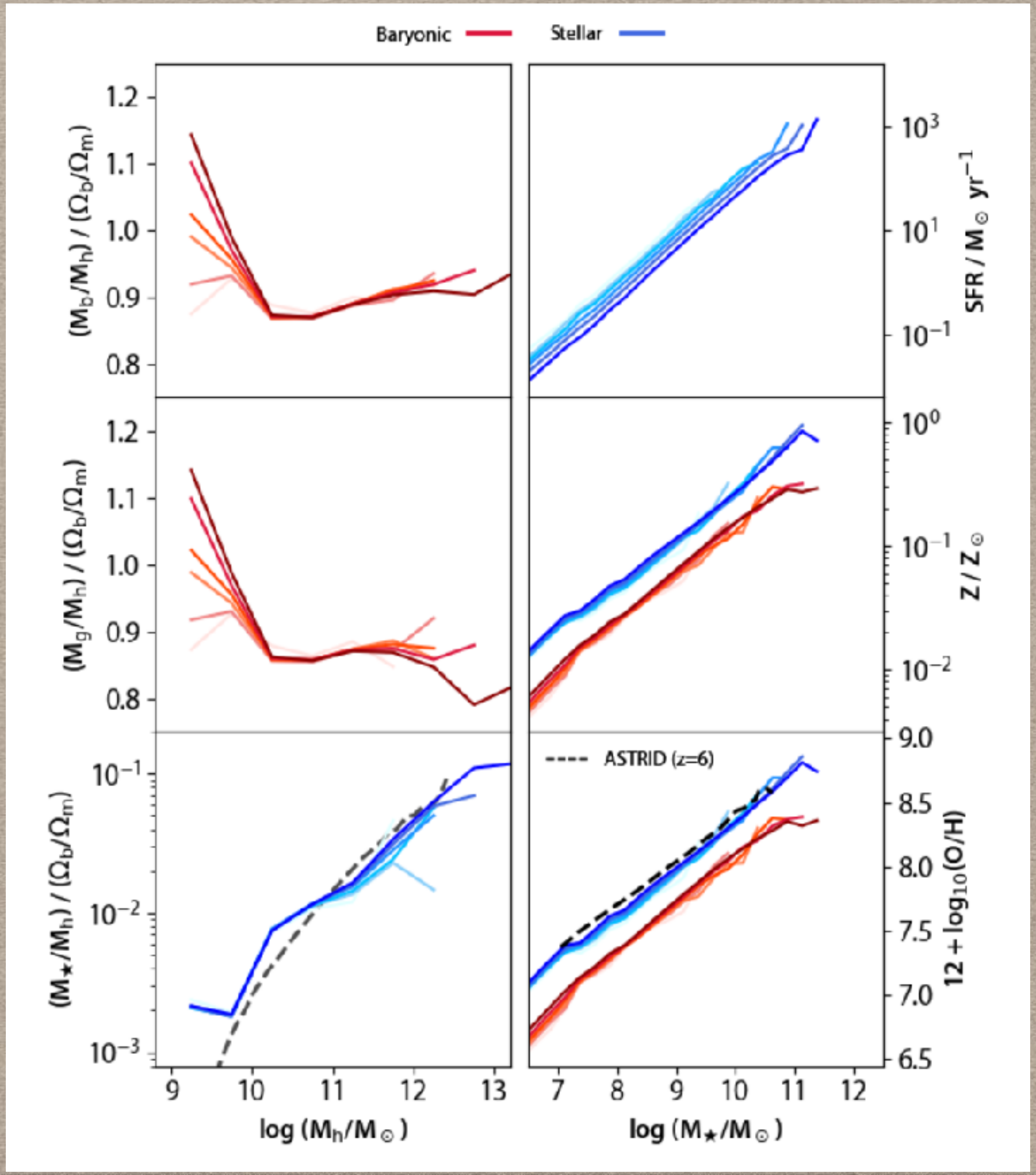

BLACKHOLE MASS FUNCTION AT Z = 0

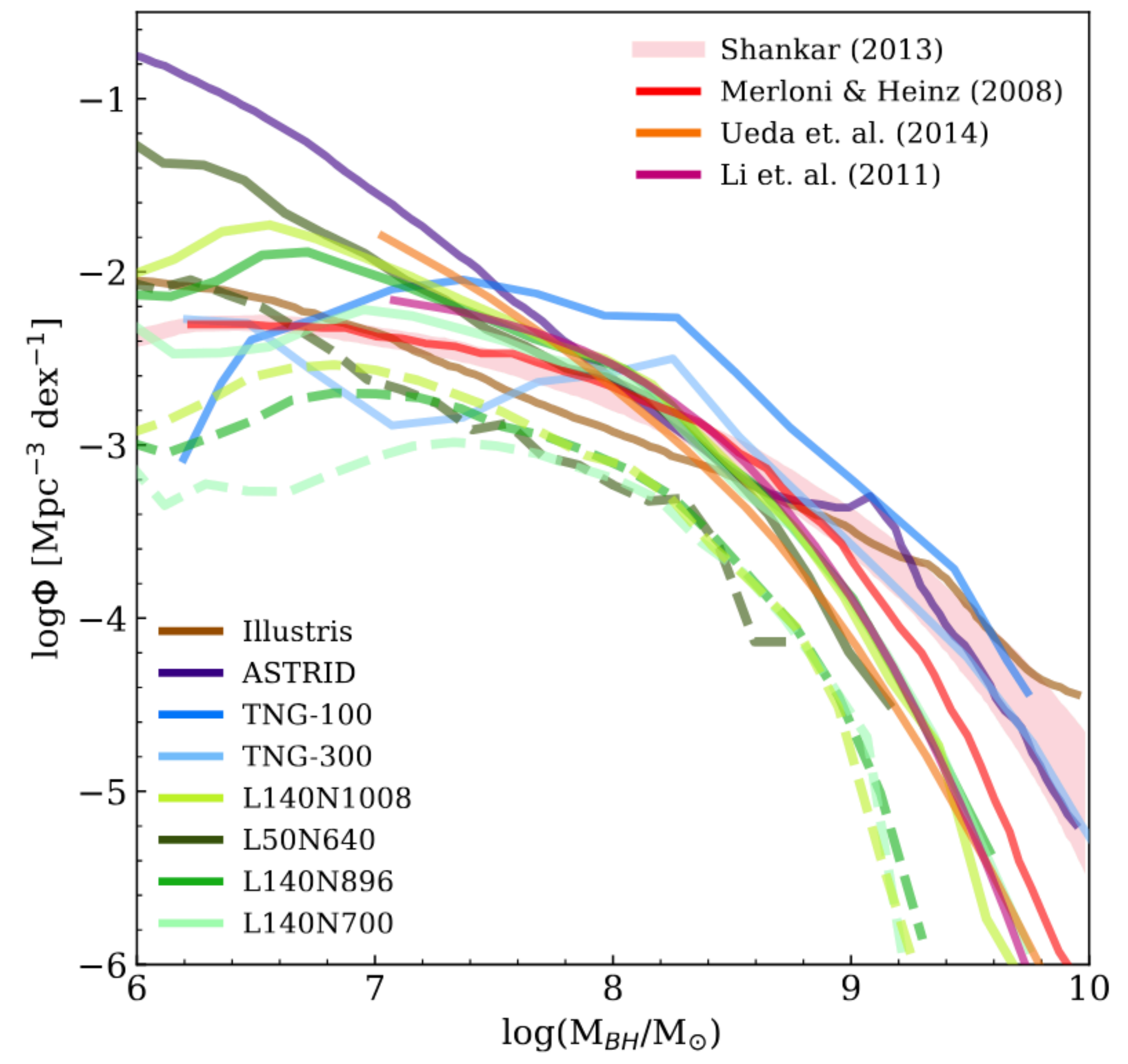

Figure 2. Comparison of the black hole mass function for different simulation volumes of **NINJA** with other simulations and observations at $z = 0$. The green lines represent the results of the **NINJA** runs (solid for centrals and dashed for satellites), the solid blue, brown and purple lines represent the results from **TNG** (Habouzit et al. 2021), **Illustris** (Sijacki et al. 2015), and the **Astrid** (Wang et al. 2025) simulations. The pink shaded region and the red, orange and magenta lines are observational constraints from Shankar (2013), Merloni & Heinz (2008), Ueda et al. (2014), and Li et al. (2011) respectively. The error estimates from Merloni & Heinz (2008) are extremely small and have not been included. The pink shaded region of Shankar (2013) represents the 1σ uncertainty of the mass function assuming the $M_{\rm BH} - \sigma$ relation from McConnell & Ma (2013).

Magare et al. 2025, arxiv

LIGHT GENERATION

$$F_\lambda(z) = \sum_{\mathrm{i}=1}^{\mathrm{i}=N} \left(\frac{m_i}{10^6 M_\odot}\right) [f_\lambda^{\mathrm{st}} \left(\tau_i(z), Z_i^{\mathrm{birth}}\right) + f_\lambda^{nb} \left(\tau_i(z), Z_i^{\mathrm{birth}}\right)]. \tag{8}$$

Here f_λ^{st} and f_λ^{nb} are the contributions of the stellar and nebular emission obtained for an ith star particle of mass m_i and age $\tau_i(z) = t_i(z) - t_i^{\mathrm{birth}}$ where $t_i(z)$ is the time of snapshot (corresponding to age of the Universe in the given cosmology) at redshift z.The t_i^{birth} and Z_i^{birth} are birth time and inherited birth metallicity respectively. [redacted]

SSP EVOLUTION

- Salpeter IMF.
- 10^6 $M_\odot$ single burst.
- $Z = 1/20\ Z_\odot$.
- "STARBURST99"
- Metallicity, Binary fraction, IMF, mass cut-offs will affect the computed spectrum.

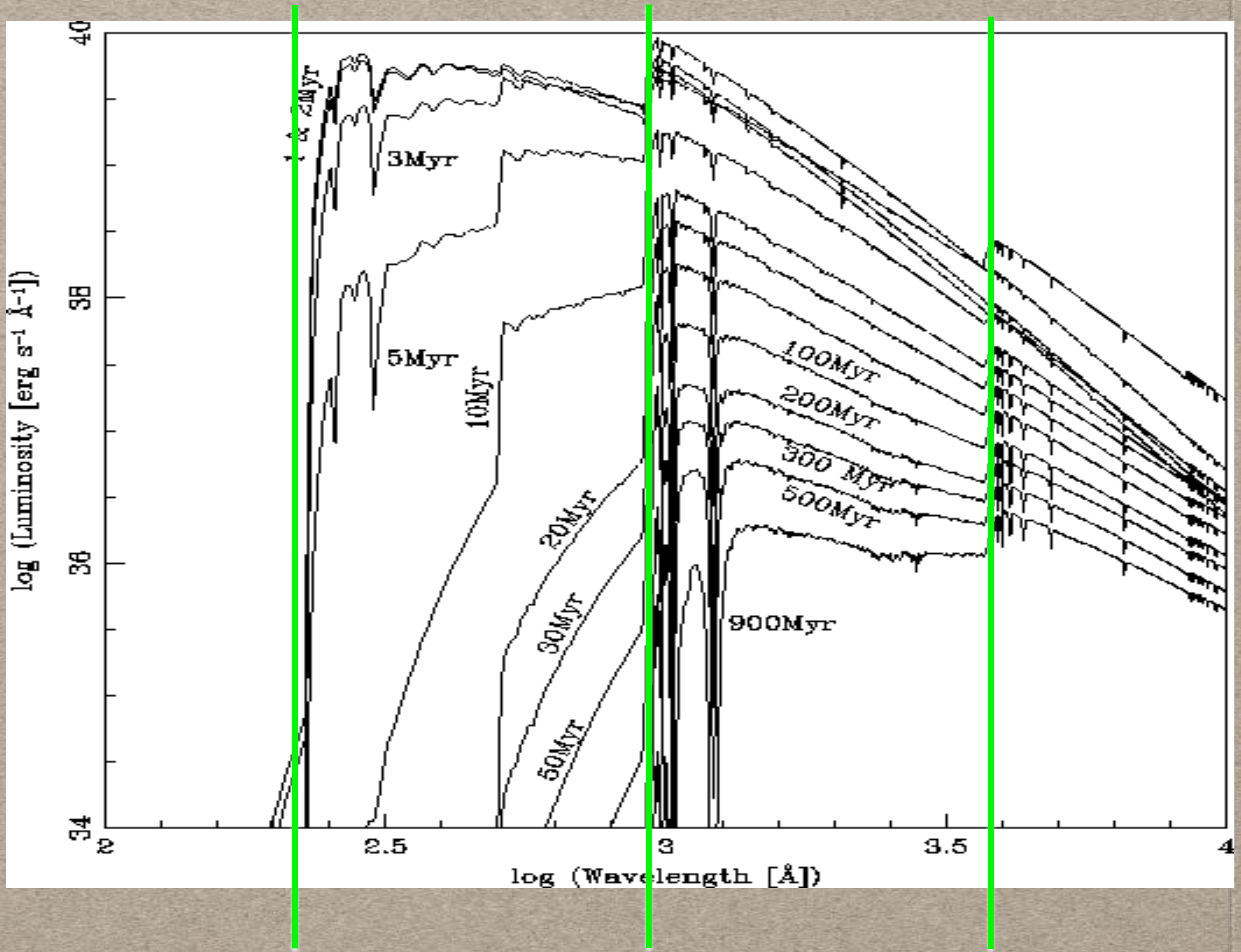

LIGHT GENERATION - IMF

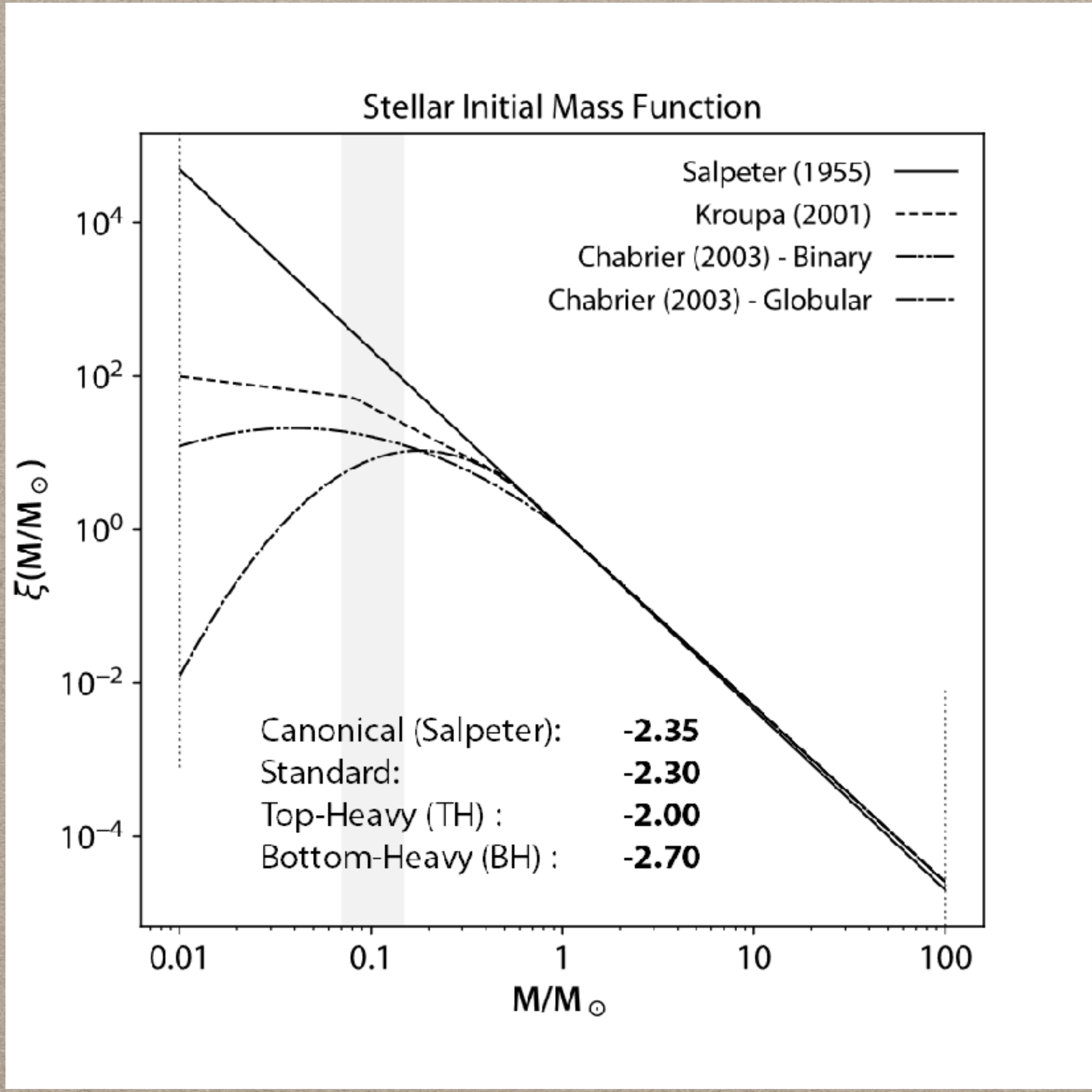

- Brightness in UV depends on fraction of massive stars formed for a given star formation rate.
- IMF is also used for metal production and SNe feedback (our default is Chabrier IMF).

LIGHT GENERATION: NEBULAR EMISSION

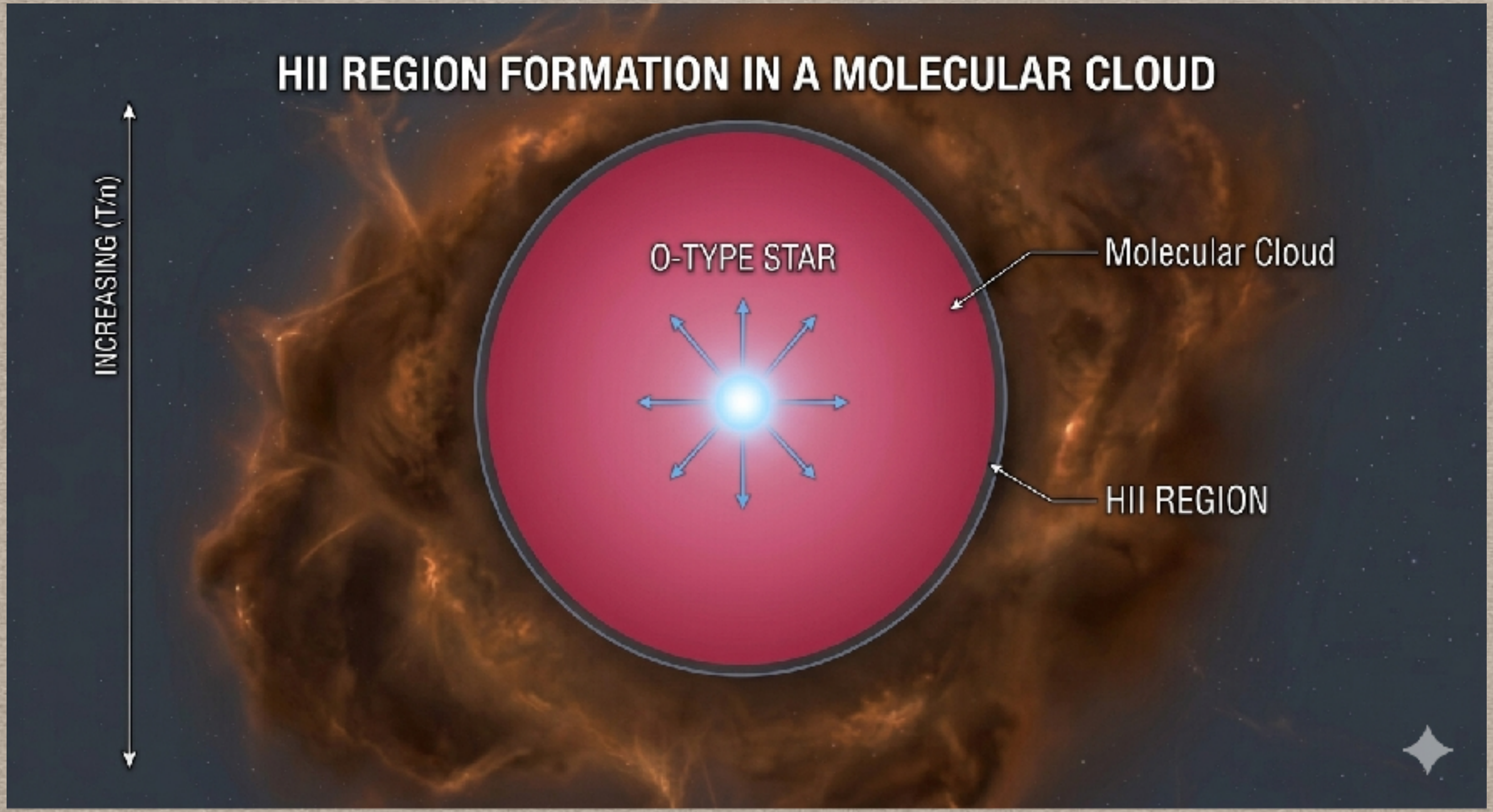

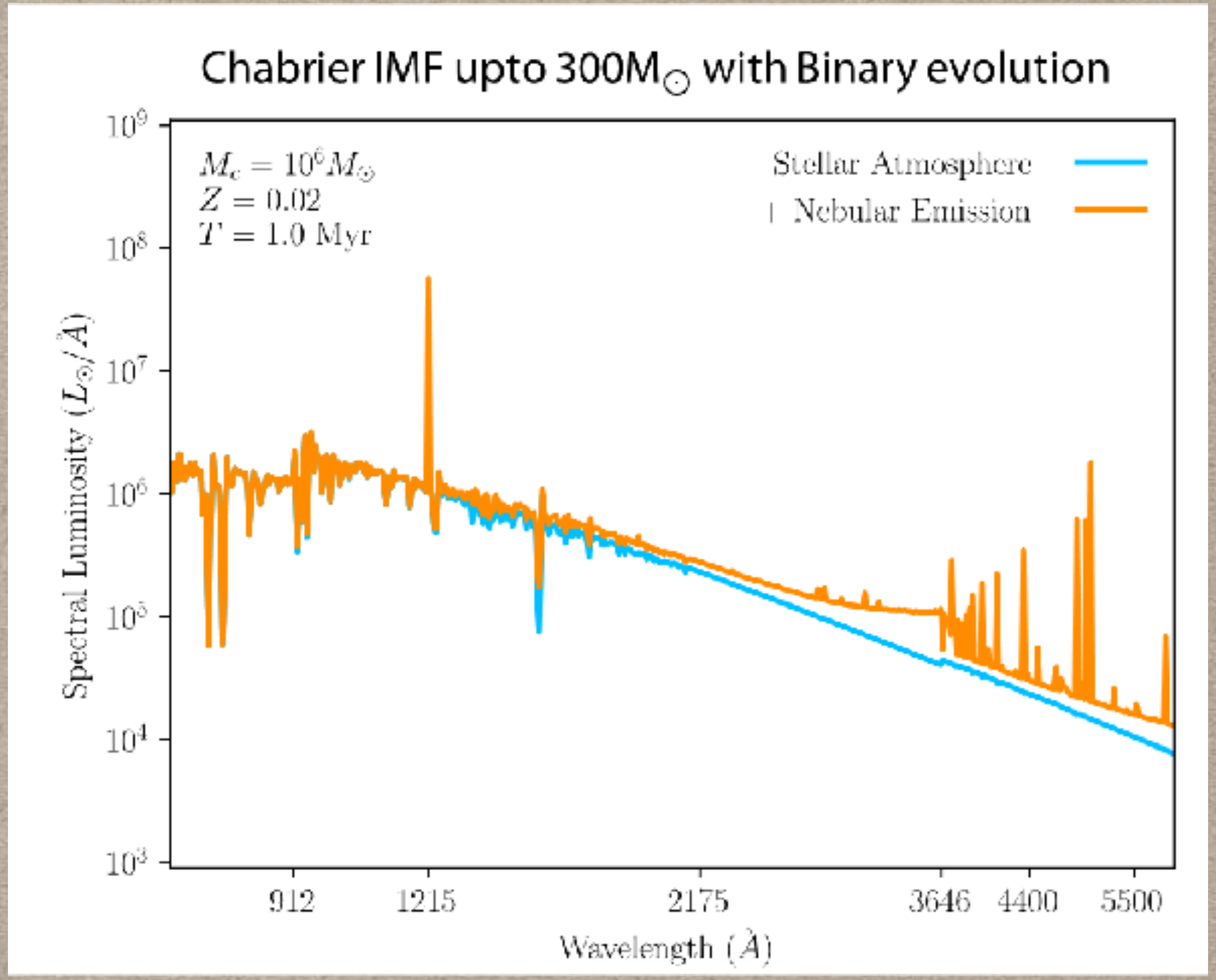

- Since expected HII region size is very small compared to our spatial resolution this is usually modelled as sub-grid physics using cloudy.
- Parameters are : density, covering factor, matter/radiation bound assumption.

NEED FOR DUST EXTINCTION

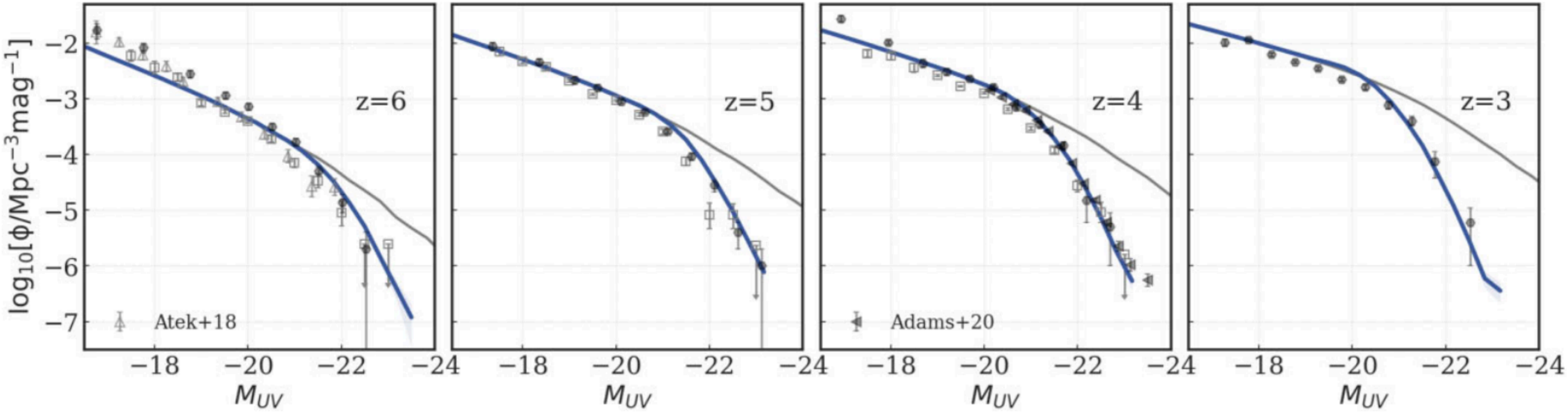

Figure 3. Galaxy UVLFs. Data points with error bars give the current observational results collected from Bouwens et al. (2015), Atek et al. (2015, 2018), Finkelstein et al. (2015), Bhatawdekar et al. (2019), Stefanon et al. (2019), Adams et al. (2020), Bowler et al. (2020), and Bouwens et al. (2021). The grey dashed lines are the intrinsic UV luminosity of the FOF groups. The grey solid lines are the intrinsic UV luminosity for the identified SUBFIND galaxies. The blue lines are the galaxy UV luminosity corrected for dust extinction.

Bird et al., 2022, MNRAS, 512, 3703

DUST ABUNDANCE

Li et al.

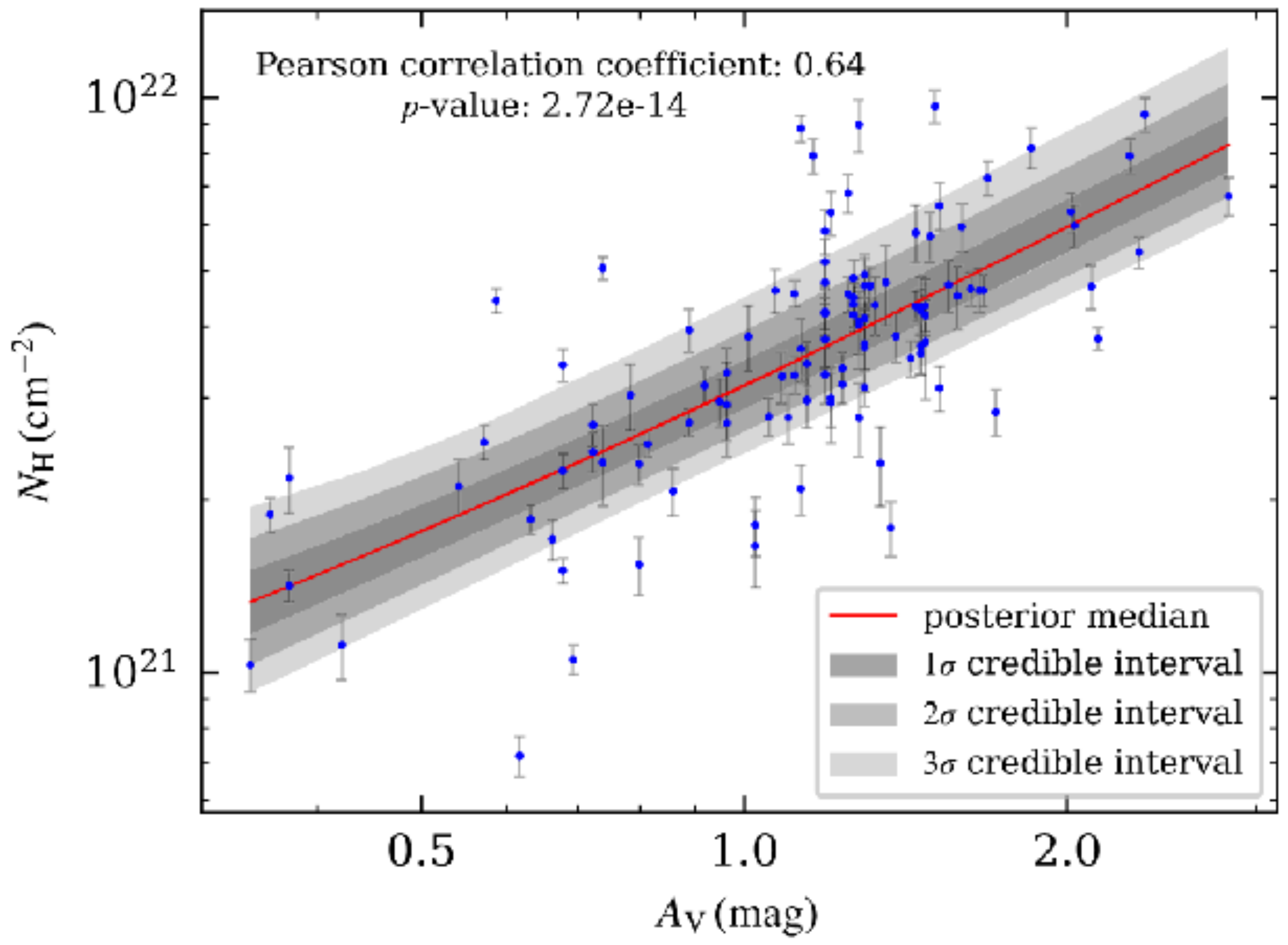

Figure 9. Best-fit correlation between the column density of hydrogen nuclei N_H and visual dust extinction A_V for the 112 strongly correlated dust-CO clouds, yielding an average GDR value of $(2.80^{+0.37}_{-0.34}) \times 10^{21}\ cm^{-2}\ mag^{-1}$. The best-fit GDR is represented by the red line, while the corresponding different credible intervals are depicted by the gray shading.

$$N(\mathrm{H}) = \kappa \epsilon f(Z_g) A_V$$

Table 1
Comparisons of N_H/A_V from the Literature Values

Reference	N_H/A_V ($10^{21}\ cm^{-2}\ mag^{-1}$)	Comment
This study	$2.80^{+0.37}_{-0.34}$	H I and CO emission lines from 112 strongly correlated dust-CO clouds within $\|b\| \leqslant 10°$
T. Güver & F. Özel (2009)	2.21 ± 0.09	X-ray absorbing column densities toward 22 SNRs with $E(B-V) \lesssim 10$ mag
D. R. Foight et al. (2016)	2.87 ± 0.12	X-ray absorbing column densities toward 17 SNRs with $E(B-V) \lesssim 10$ mag
H. Liszt (2014a)	2.68	Only H I emission line from Galactic latitudes $\|b\| \gtrsim 20°$ and $E(B-V) \lesssim 0.1$ mag
B.-Q. Chen et al. (2015)	2.41 ± 0.01	H I and CO emission lines from the Galactic anticenter $\|b\| \gtrsim 10°$ and $E(B-V) \lesssim 1$ mag
H. Zhu et al. (2017)	2.47 ± 0.04	X-ray absorbing column densities toward 19 SNRs and 29 X-ray binaries
D. Lenz et al. (2017)	2.84	Only H I emission line in the low-column-density regime with $E(B-V) \approx 45$ mmag
H. Nguyen et al. (2018)	3.03 ± 0.52	H I absorption line from purely atomic sight lines at $\|b\| > 5°$
J. M. Shull & G. V. Panopoulou (2024)	3.32 ± 0.13	H I emission, H_2 far-UV absorption lines toward 51 quasars and gas at $\|v_{LSR}\| \leqslant 600\ km\ s^{-1}$
J. M. Shull & G. V. Panopoulou (2024)	2.97 ± 0.10	H I emission, H_2 far-UV absorption lines toward 51 quasars and gas at $\|v_{LSR}\| \leqslant 90\ km\ s^{-1}$

Note. For the literature values listed here, $E(B-V)$ is converted to A_V using $R_V = 3.1$.

- N(H)/A_V = 3.25 x 10^21 (LMC)
- N(H)/A_V = 7.40 x 10^21 (SMC-wing)
- N(H)/A_V = 13.18 x 10^21 (SMC-core)

DUST TO GAS AS A FUNCTION OF METALLICITY

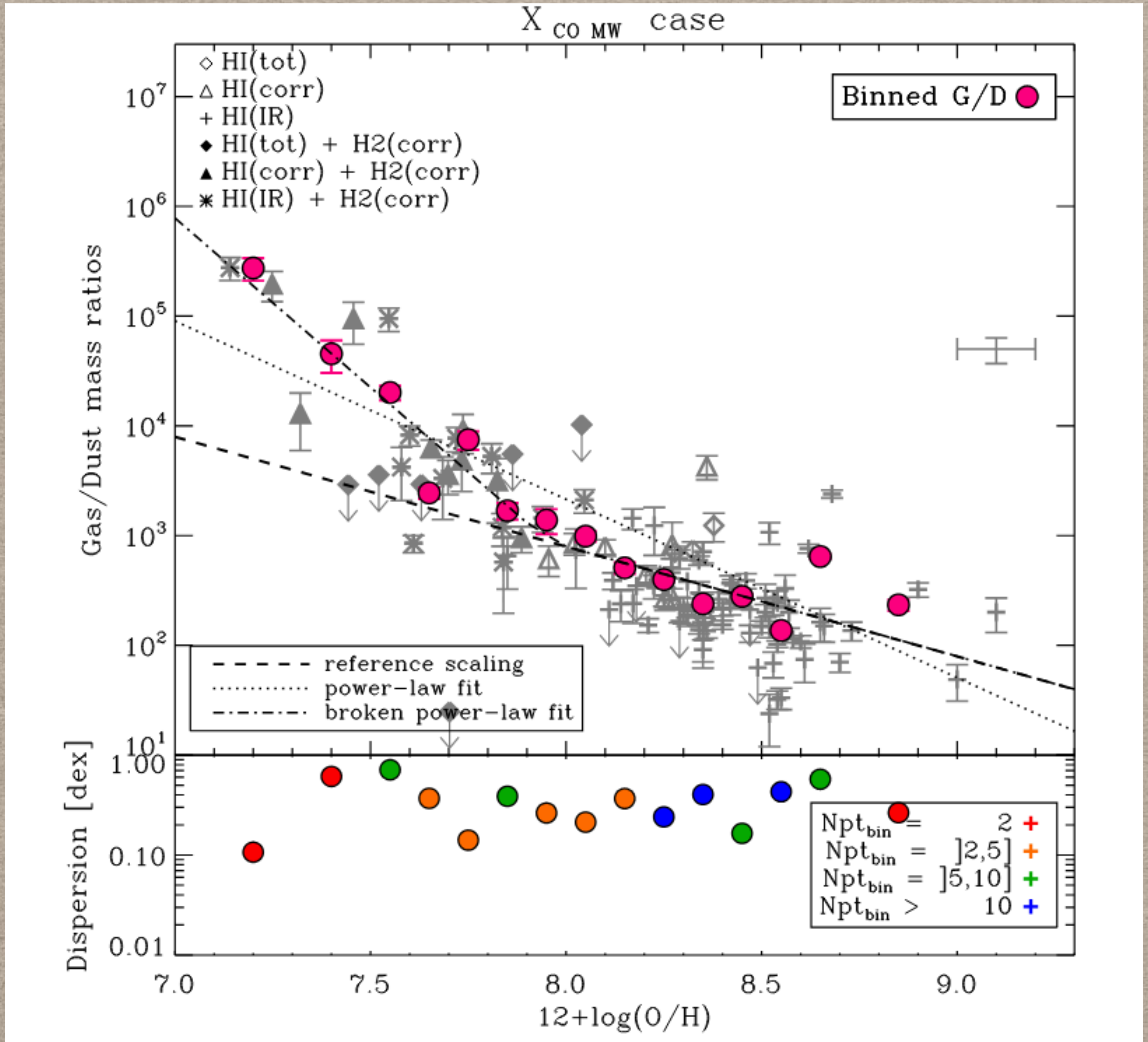

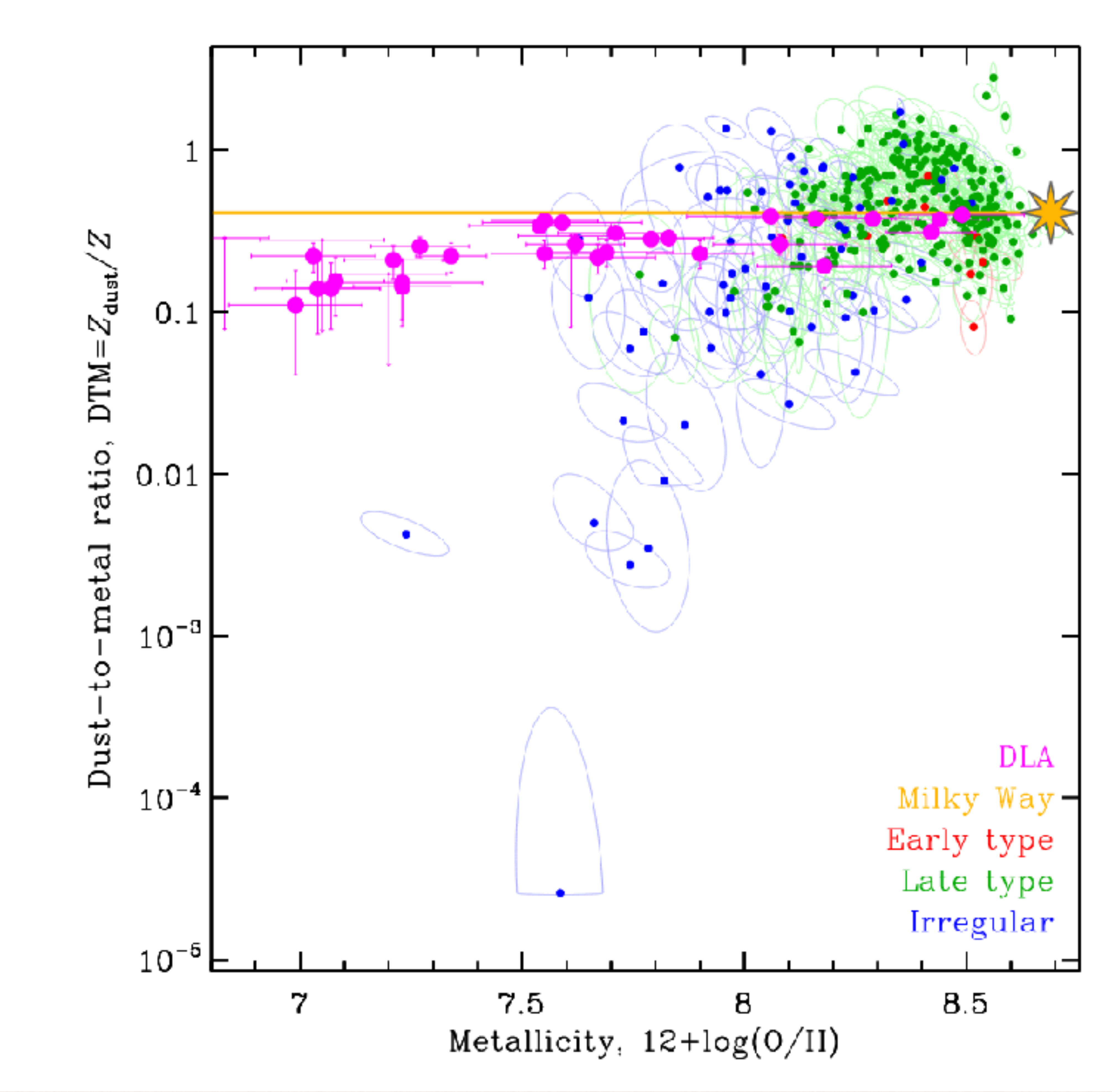

Rémy-Ruyer et al. 2014, A&A,563, A31

Galliano et al. 2021, A&A, 649, A18

EXTINCTION CURVE

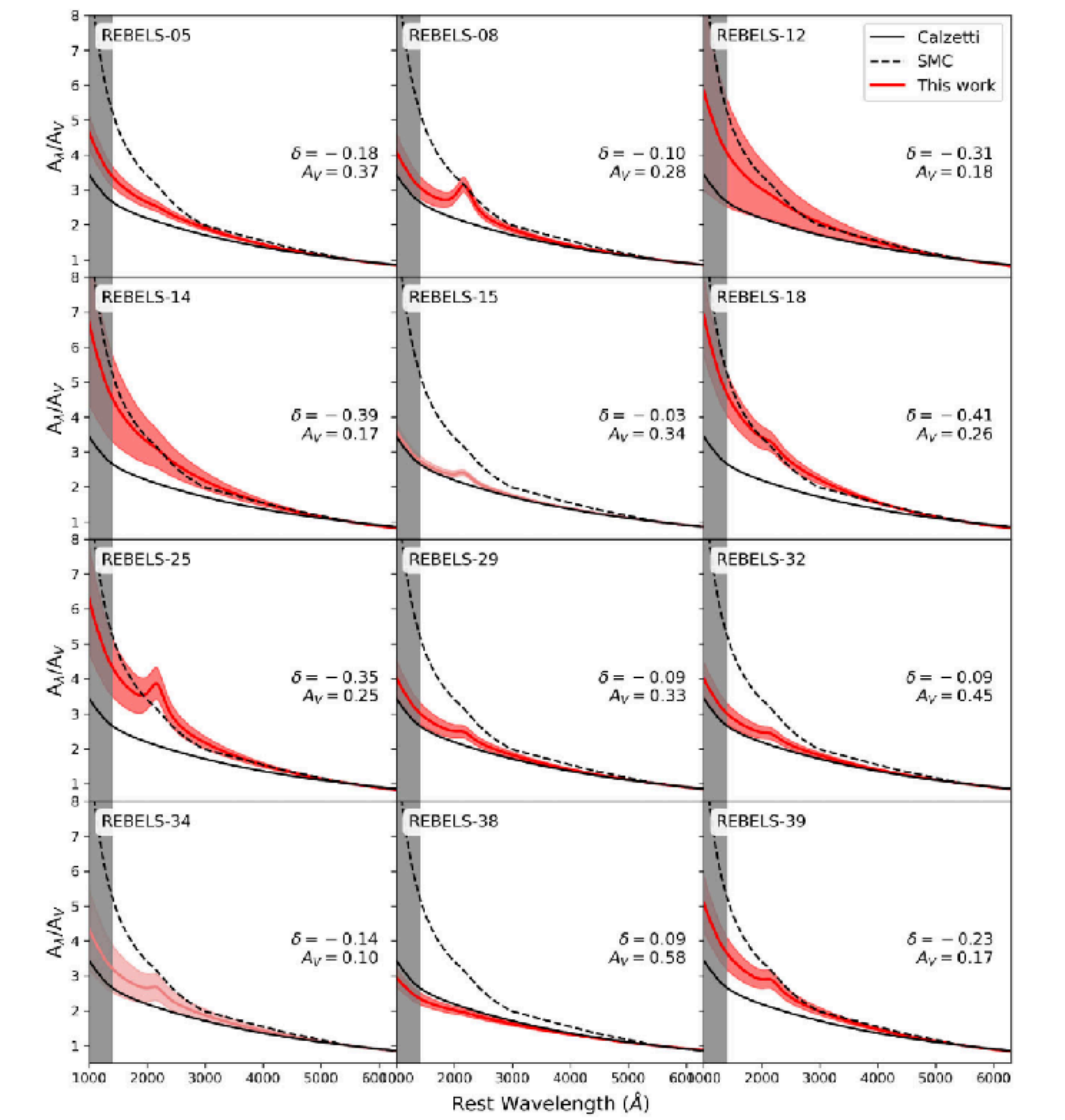

Figure 2. The best-fitting dust attenuation curves for 12 massive galaxies at $z \simeq 7$ from the REBELS-IFU program. These curves were obtained from SED fits to the global NIRSpec spectra extracted from the IFU. We use BAGPIPES to fit the SED models with an NP SFH and a Salim et al. (2018) flexible dust attenuation curve parametrization. The observed spectrum was masked below a rest wavelength of 1400 Å, as shown by the grey-shaded band. The red-shaded region shows the 1σ error on the attenuation curves. The two galaxies with no dust continuum detections (REBELS-15 and REBELS-34) are shown in a fainter shade of red. The Calzetti-like (SMC) curve is shown by the solid (dashed) black line.

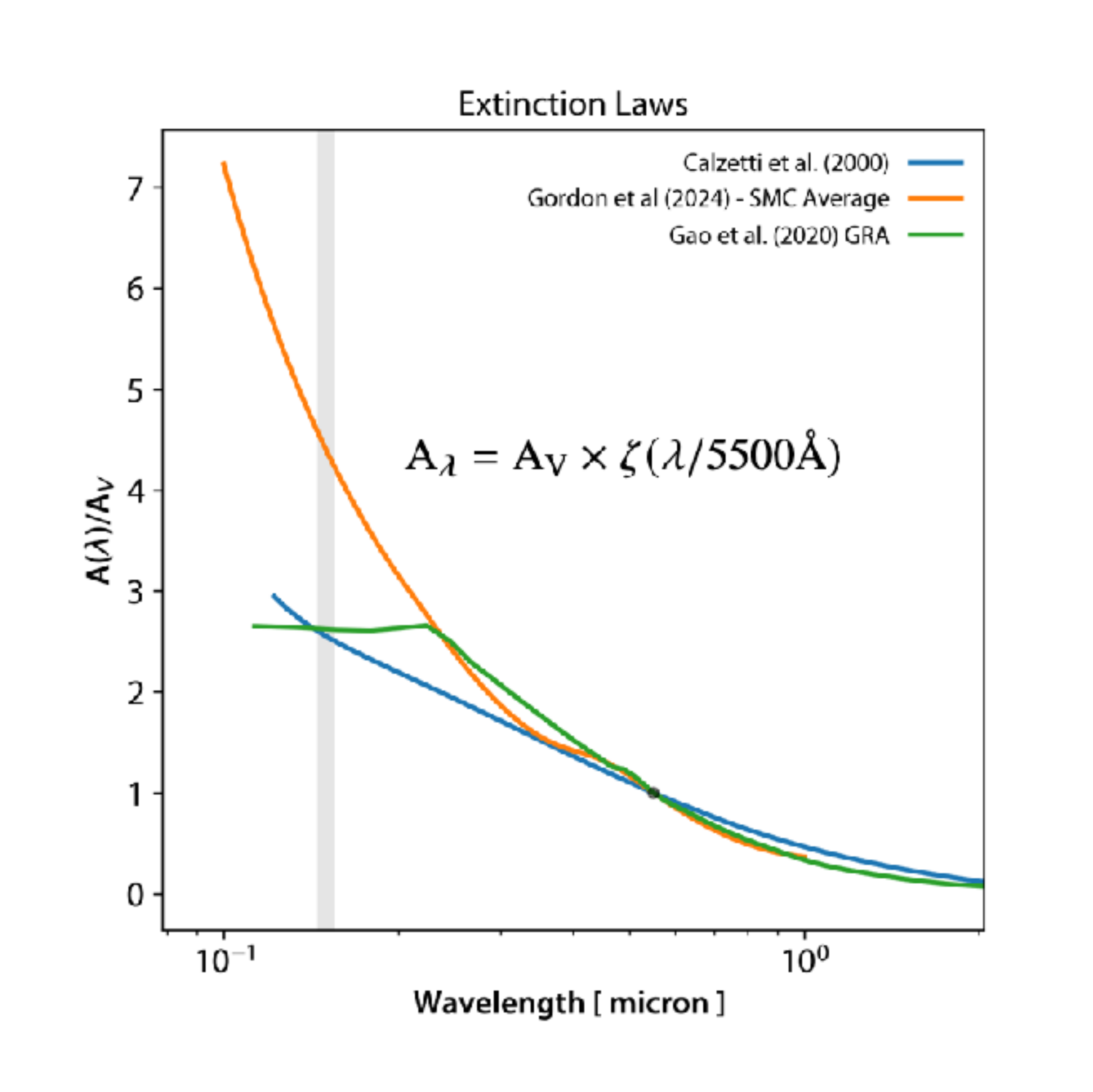

- UV spectral slope
- LF at different wavelengths

DUST ABUNDANCE

$$A_V = \frac{(1+z)^2}{\epsilon\kappa}\frac{X}{m_H}\sum_j f(Z_{g,j})^{-1}\left[\sum_i m_i W_i(r,h)\right]\Delta s_j \tag{12}$$

with

$$Z_{g,j} = \frac{\sum_i m_i Z_i W_i}{\sum_i m_i W_i}. \tag{13}$$

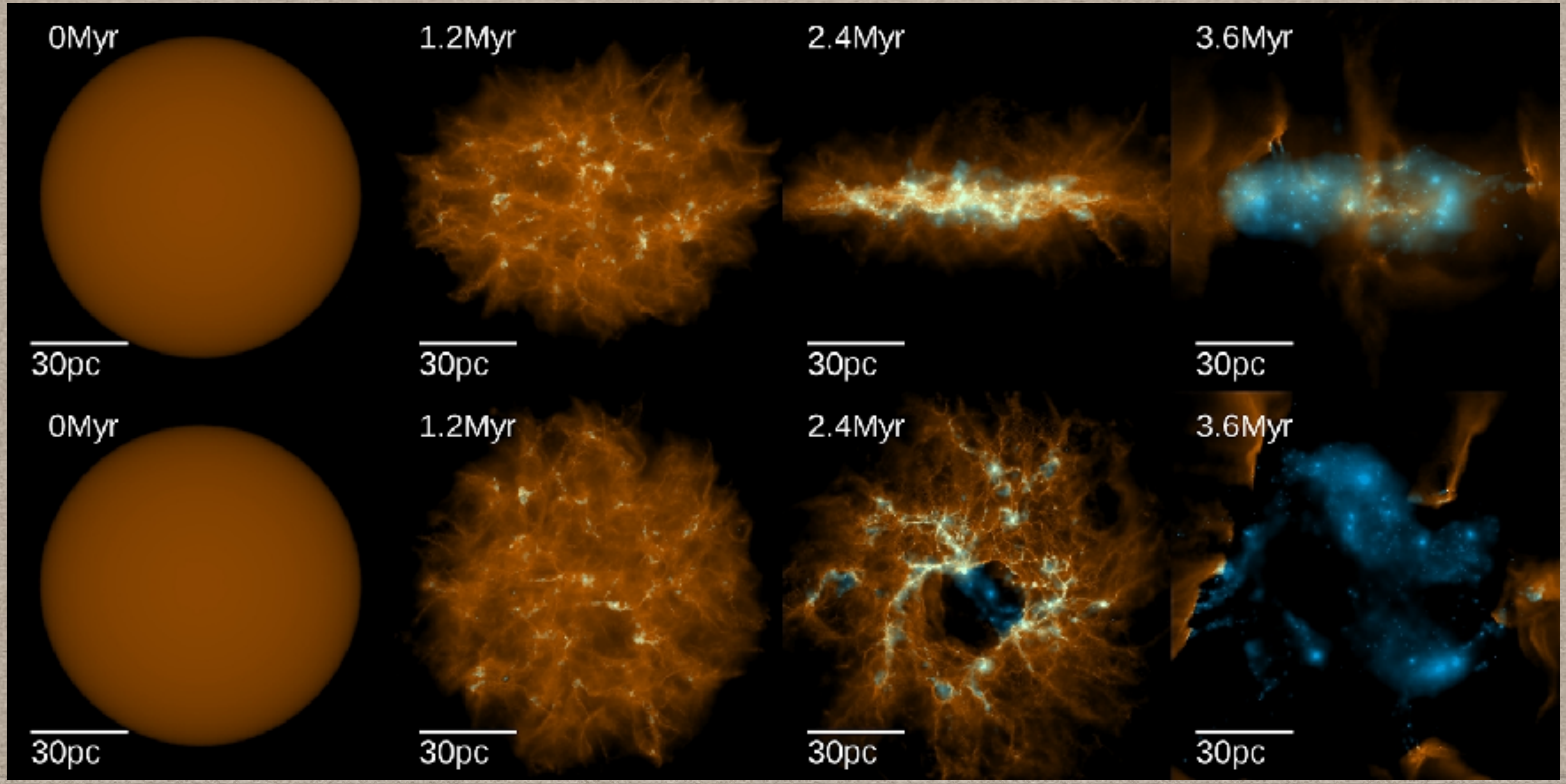

For stars younger than 20 Myr

$$A_V = A_V^{ISM} + A_V^{BC}$$

$$A_V^{BC} = 2\langle A_V^{ISM}\rangle$$

Emission lines will see different Av

SPECTRUM AFTER DUST REDDENING

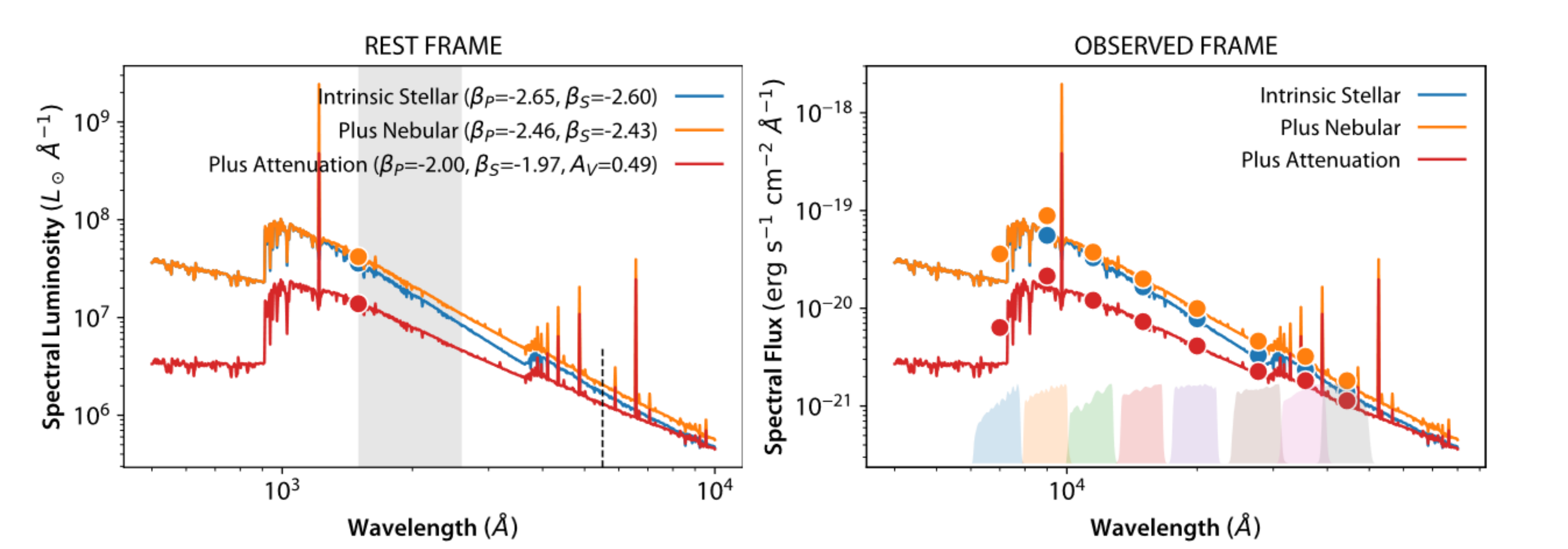

EXTINCTION: BALMER DECREMENT

$$F_{H\alpha} = F^0_{H\alpha} exp(-\tau_{6563})$$

$$F_{H\beta} = F^0_{H\beta} exp(-\tau_{4863})$$

$$\frac{F_{H\alpha}}{F_{H\beta}} = \frac{F^0_{H\alpha}}{F^0_{H\beta}} exp(-\tau_{6563} + \tau_{4863})$$

where $\frac{F^0_{H\alpha}}{F^0_{H\beta}} = 2.86$ for case-B recombination at $T = 10^4$ K.

τ_λ comes from an assumed extinction curve and E(B-V) values.

$$f^{\mathrm{i}}_\lambda(\lambda) = f_\lambda(\lambda) \cdot \exp\left(\frac{\tau_V}{\tau(V)} \cdot \tau(\lambda)\right).$$

$$\tau_V^{\mathrm{Balmer}} = \frac{\ln(\mathrm{H}\alpha/\mathrm{H}\beta) - \ln(\mathrm{H}\alpha^{\mathrm{i}}/\mathrm{H}\beta^{\mathrm{i}})}{\tau(\beta) - \tau(\alpha)} \cdot \tau(V).$$

UVLF AT Z>5: OBSERVATIONS AND PREDICTIONS OF NINJA

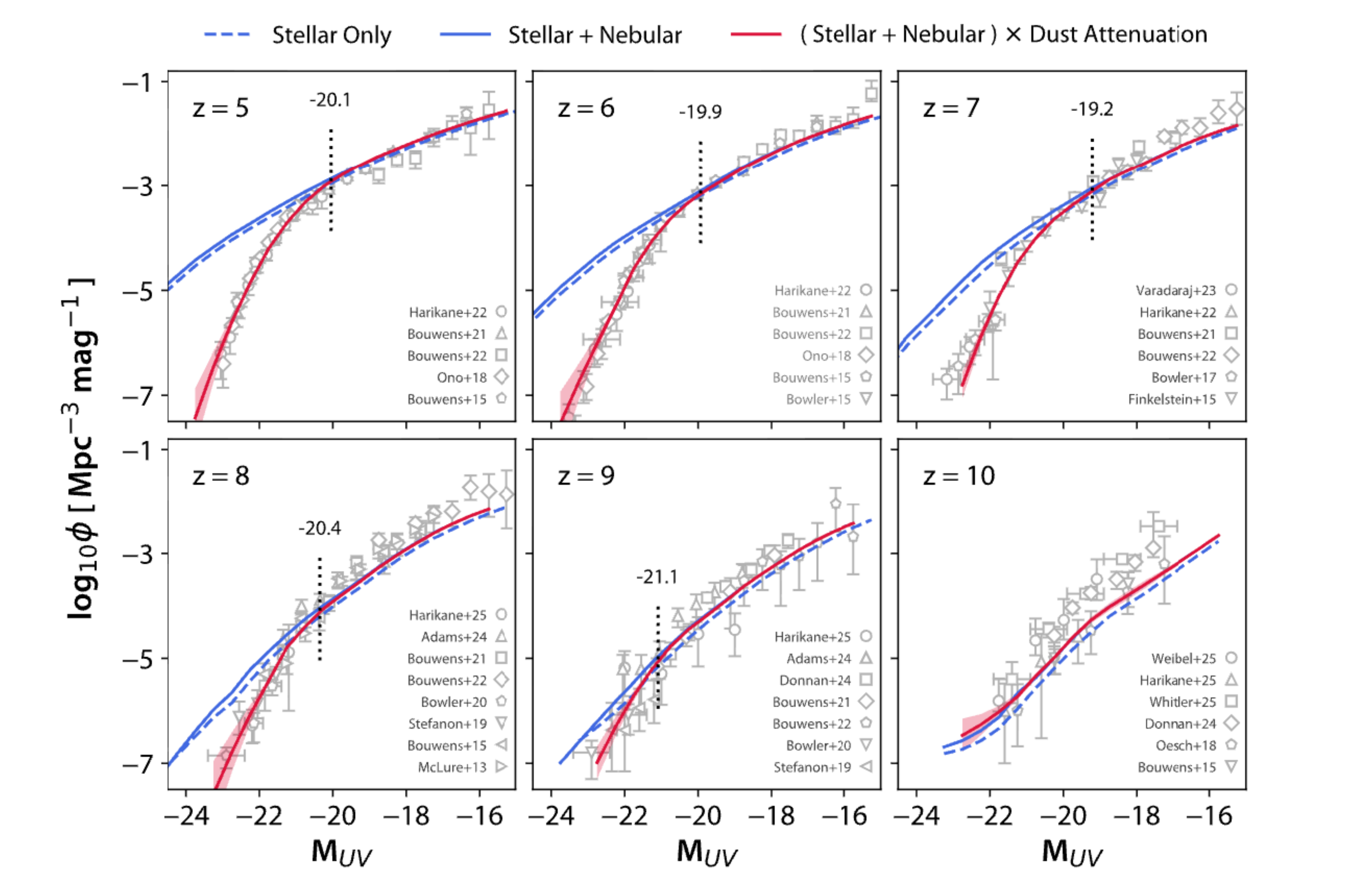

UVLF AT Z>5: OTHER SIMULATIONS AND NINJA

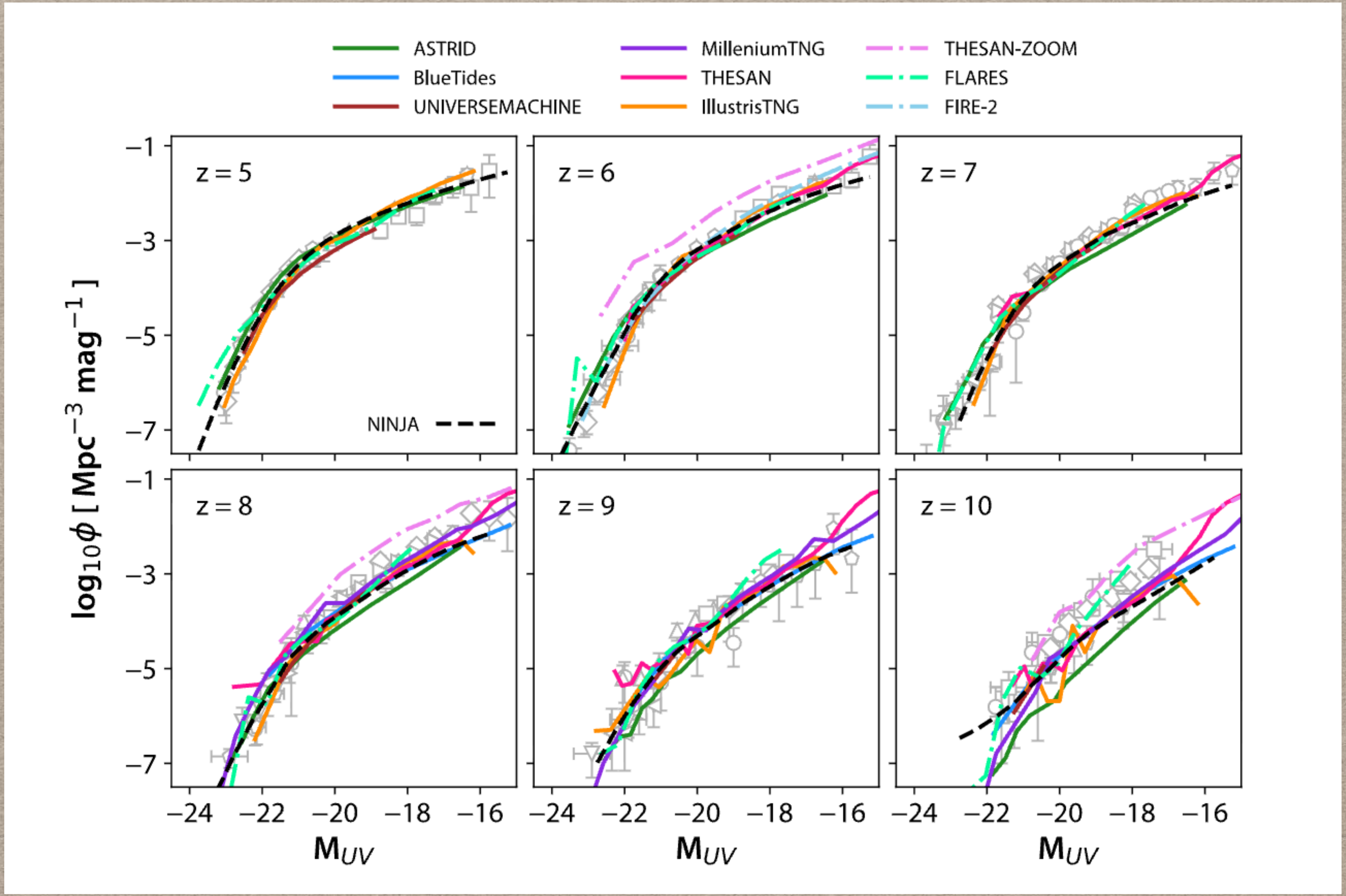

JWST: CLUSTERING OF HIGH-Z GALAXIES

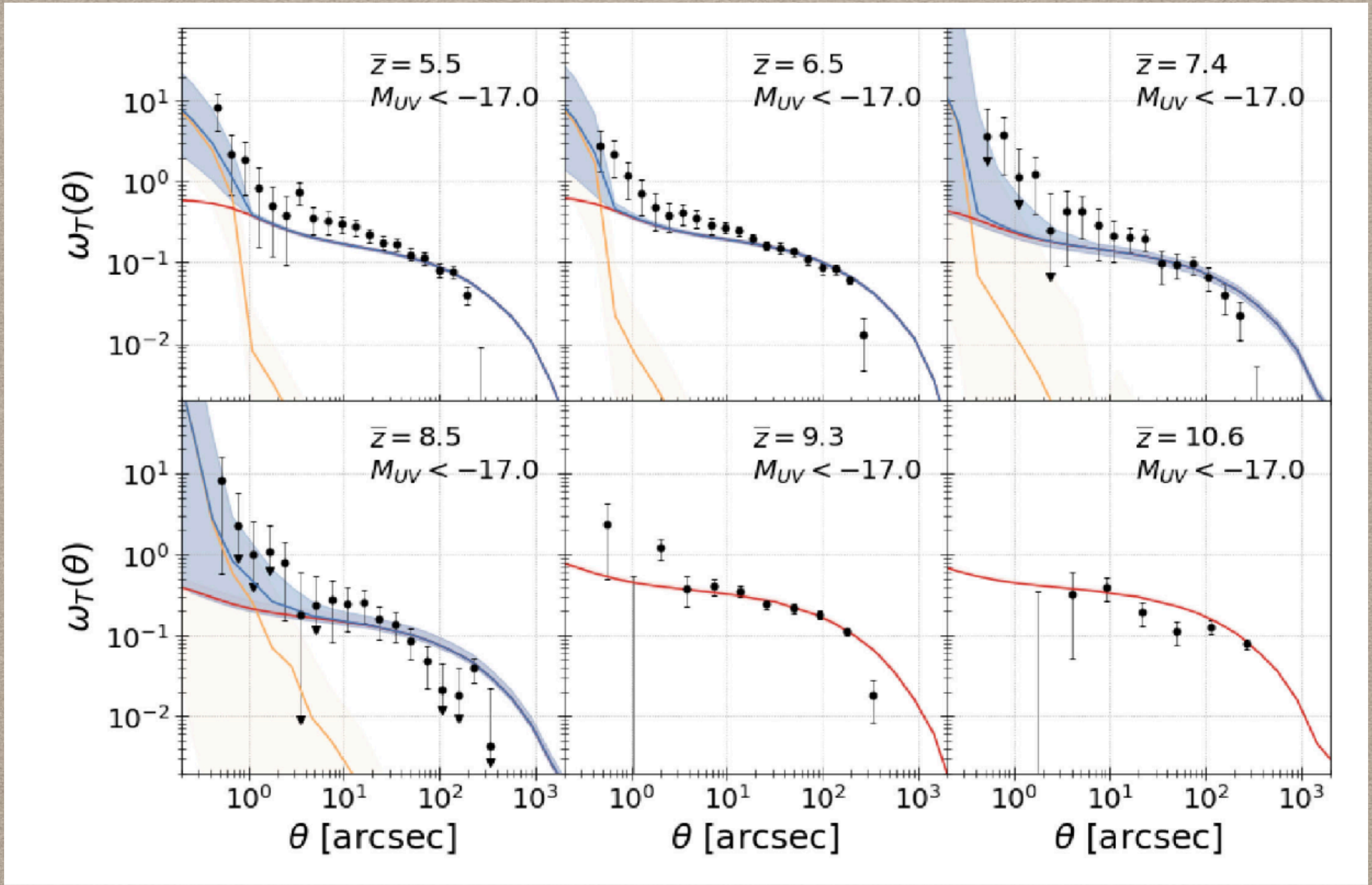

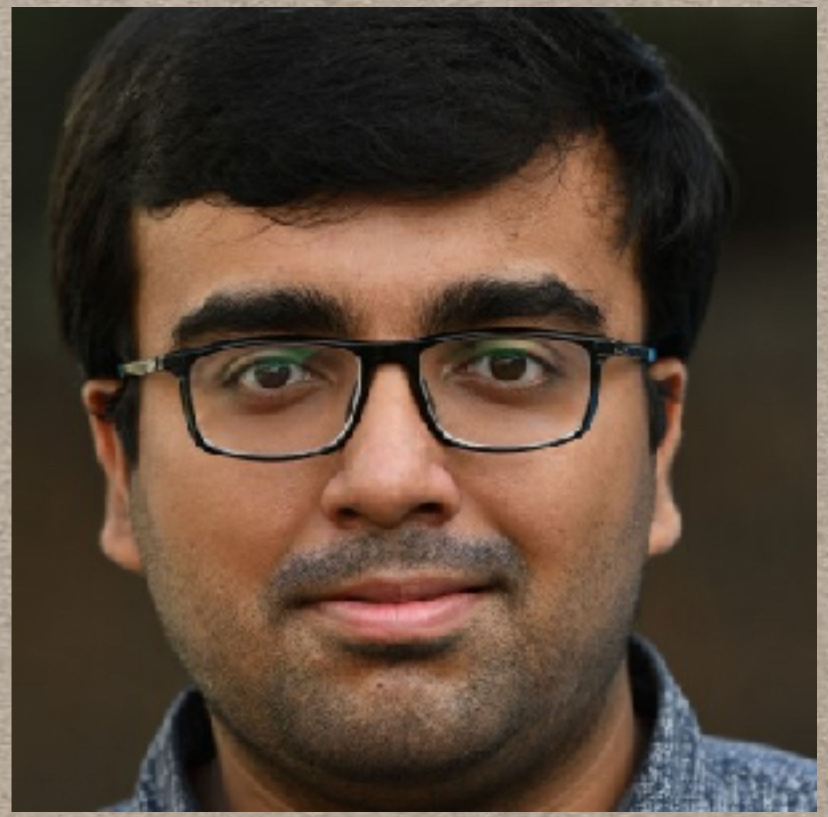

ANIRBAN

Dalmasso et al. 2026, MNRAS,546, 1

JWST DAMPING WINGS

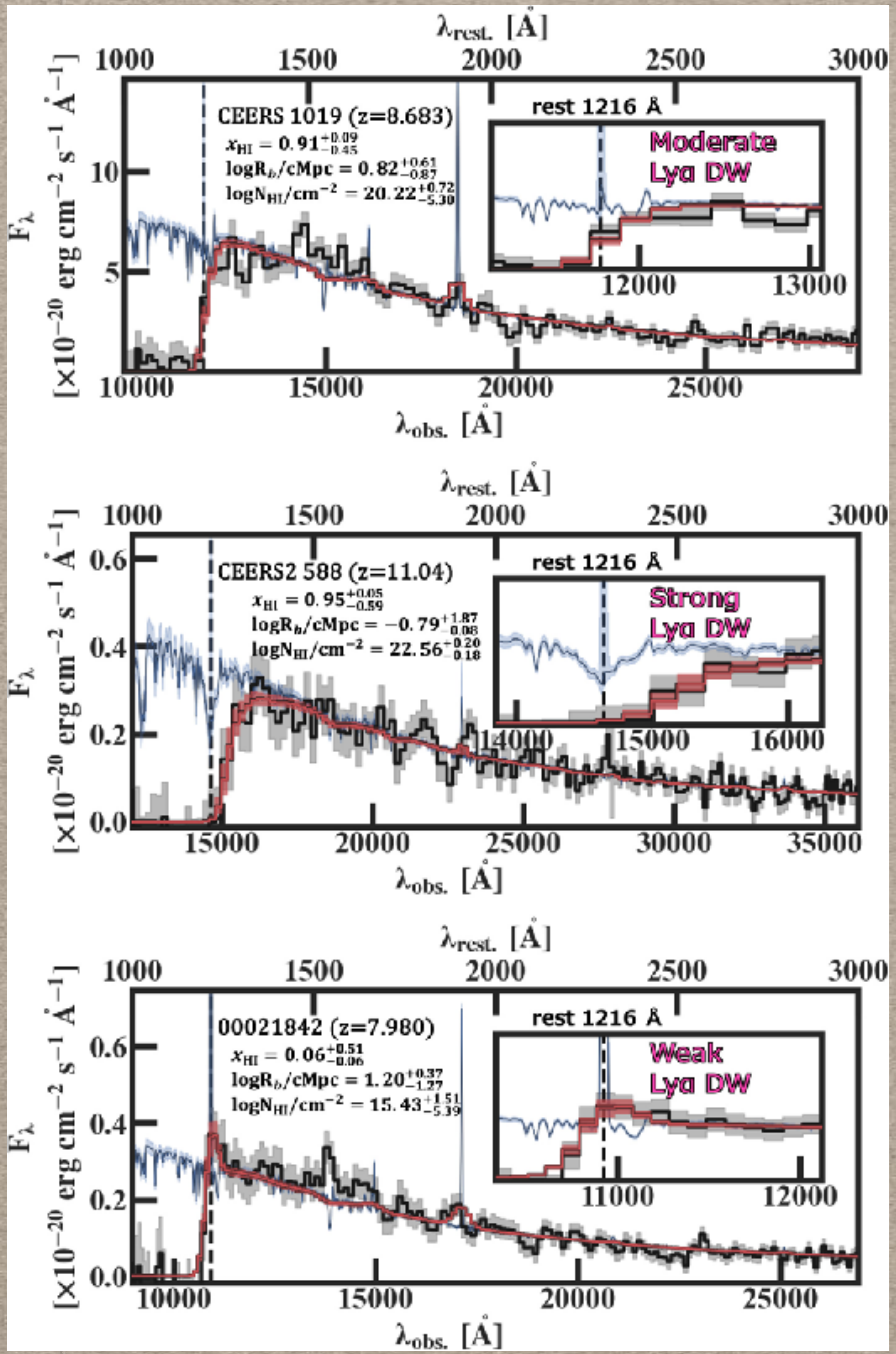

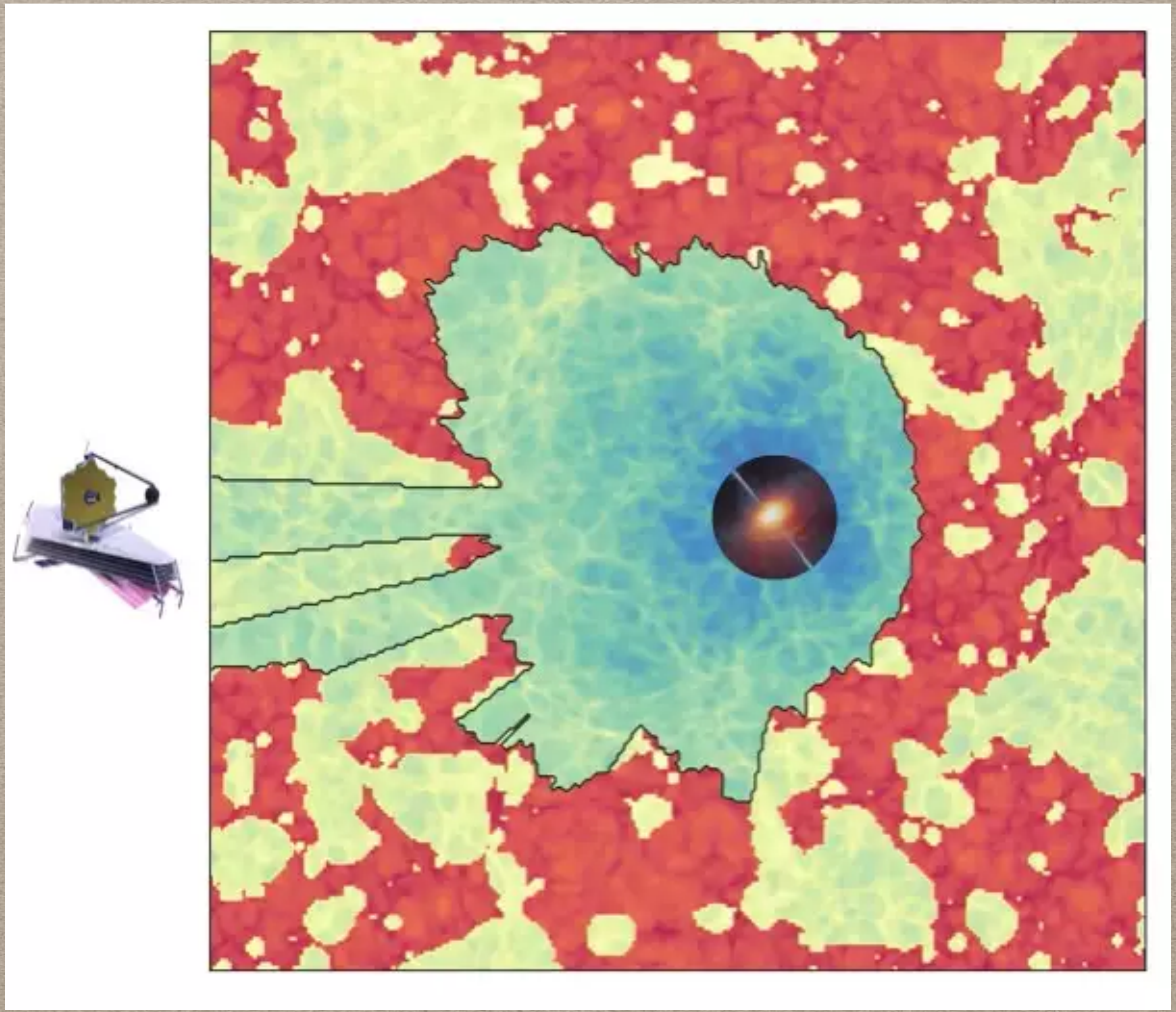

- What is the relative contribution of ISM, CGM and IGM to the damping wing?

COSMIC REIONISATION

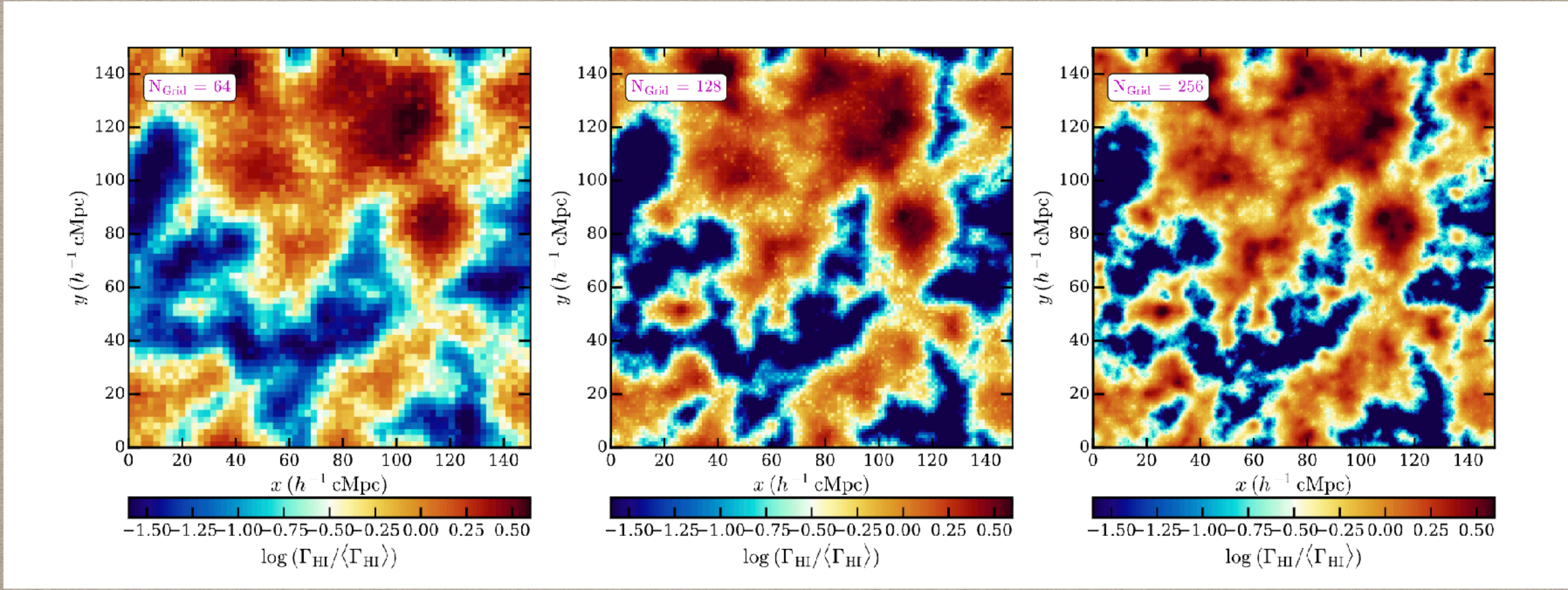

ANIRBAN, PRAKASH AND TIRTH

GALAXY SIZE EVOLUTION

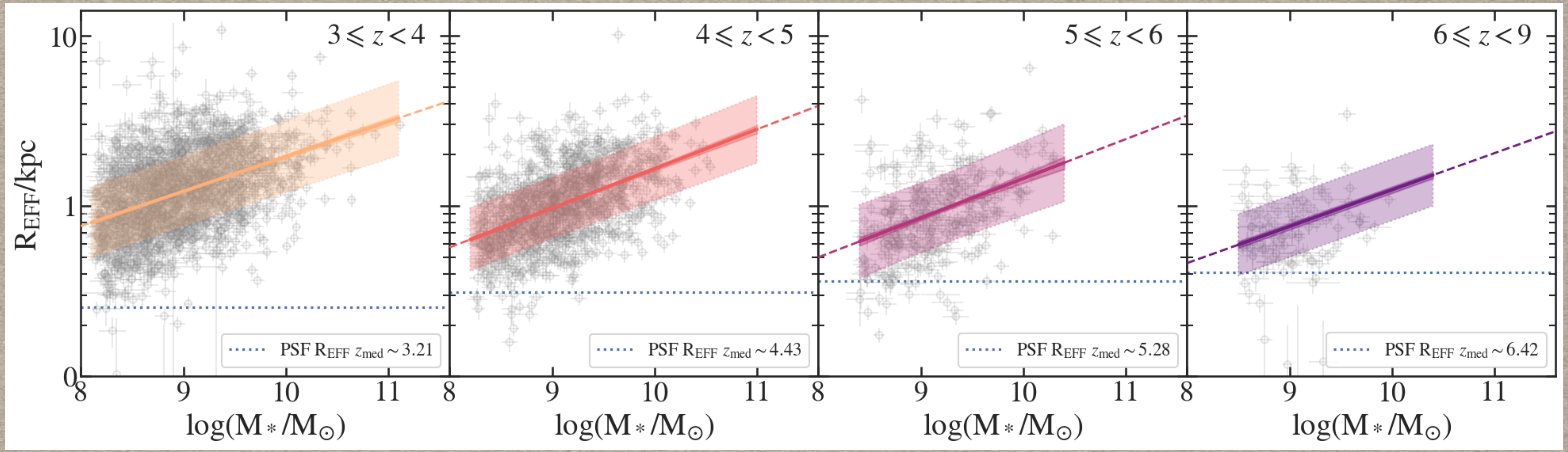

Fig. 3. Rest-optical size–mass relation across four redshift bins: $3 \leq z < 4$, $4 \leq z < 5$, $5 \leq z < 6$ and $6 \leq z < 9$. The solid black line represents the median fit, with its uncertainty in dark shading and intrinsic scatter in light grey. The grey open circles mark the data points used in the fit. The dotted line indicates the PSF size at the bin's median redshift; points below this threshold R_{EFF} were excluded from fitting. In the highest redshift bin, due to limited data, we fixed the slope and fitted only the intercept and intrinsic dispersion (see Section 3.4).

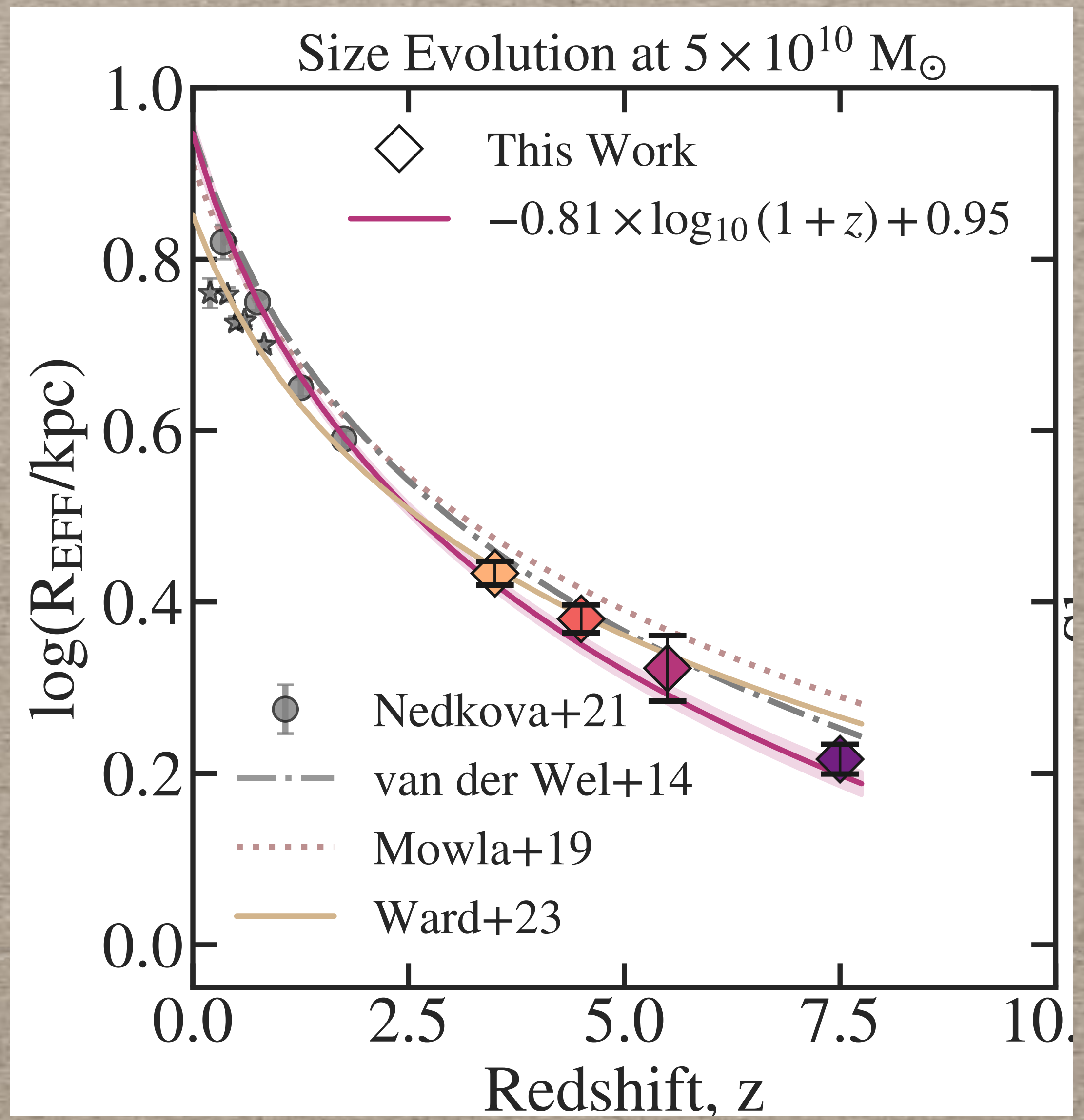

- Typical sizes are ≤ kpc for $\leq 5 \times 10^{10} M_\odot$
- Number of stars per unit volume is >100 times that of what we typically see in the local universe. Kinematics is interesting.
- Good galaxy formation model should predict the correct sizes and its redshift evolution.

IMAGE AND SED FITTING ANALYSIS

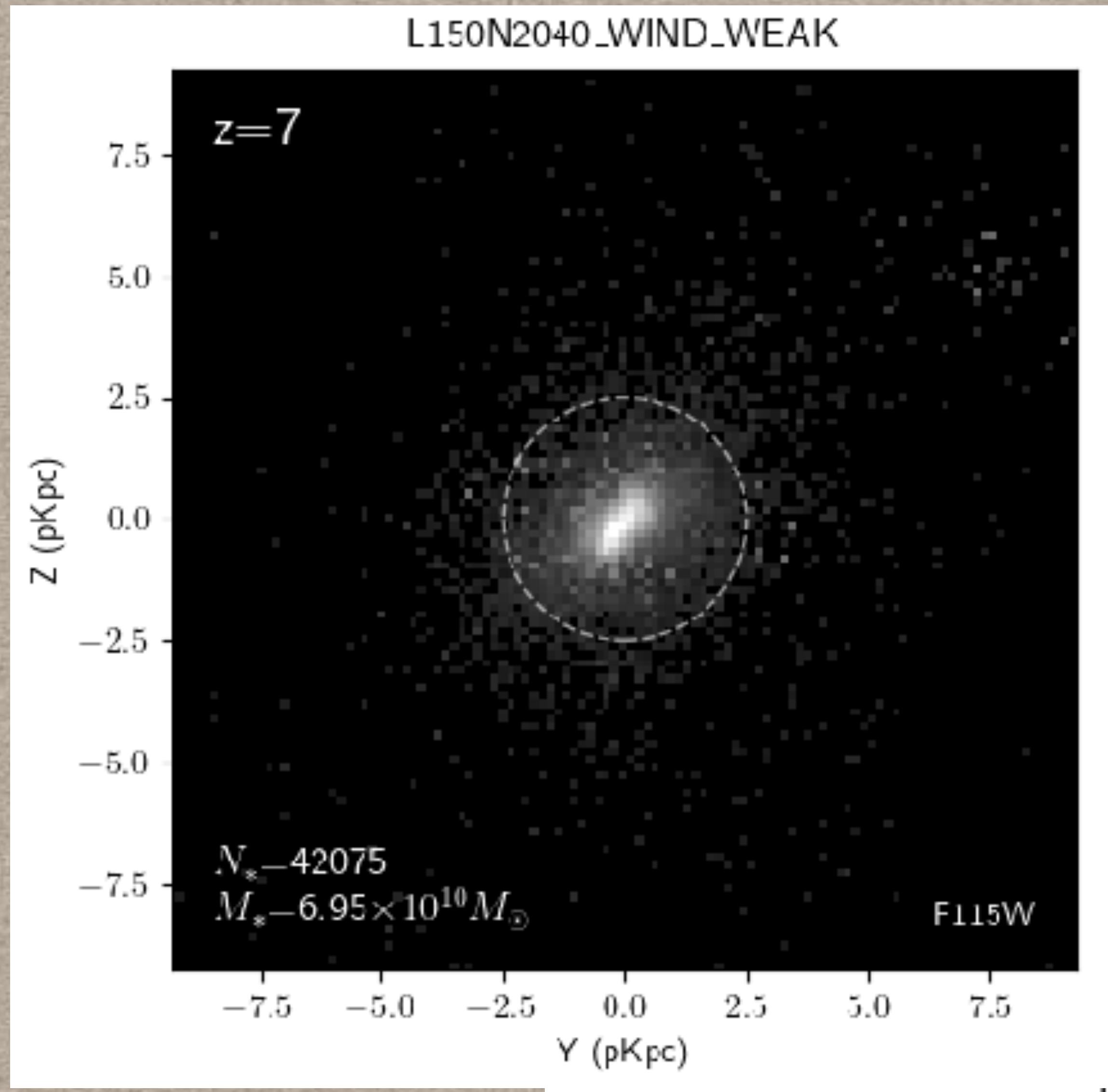

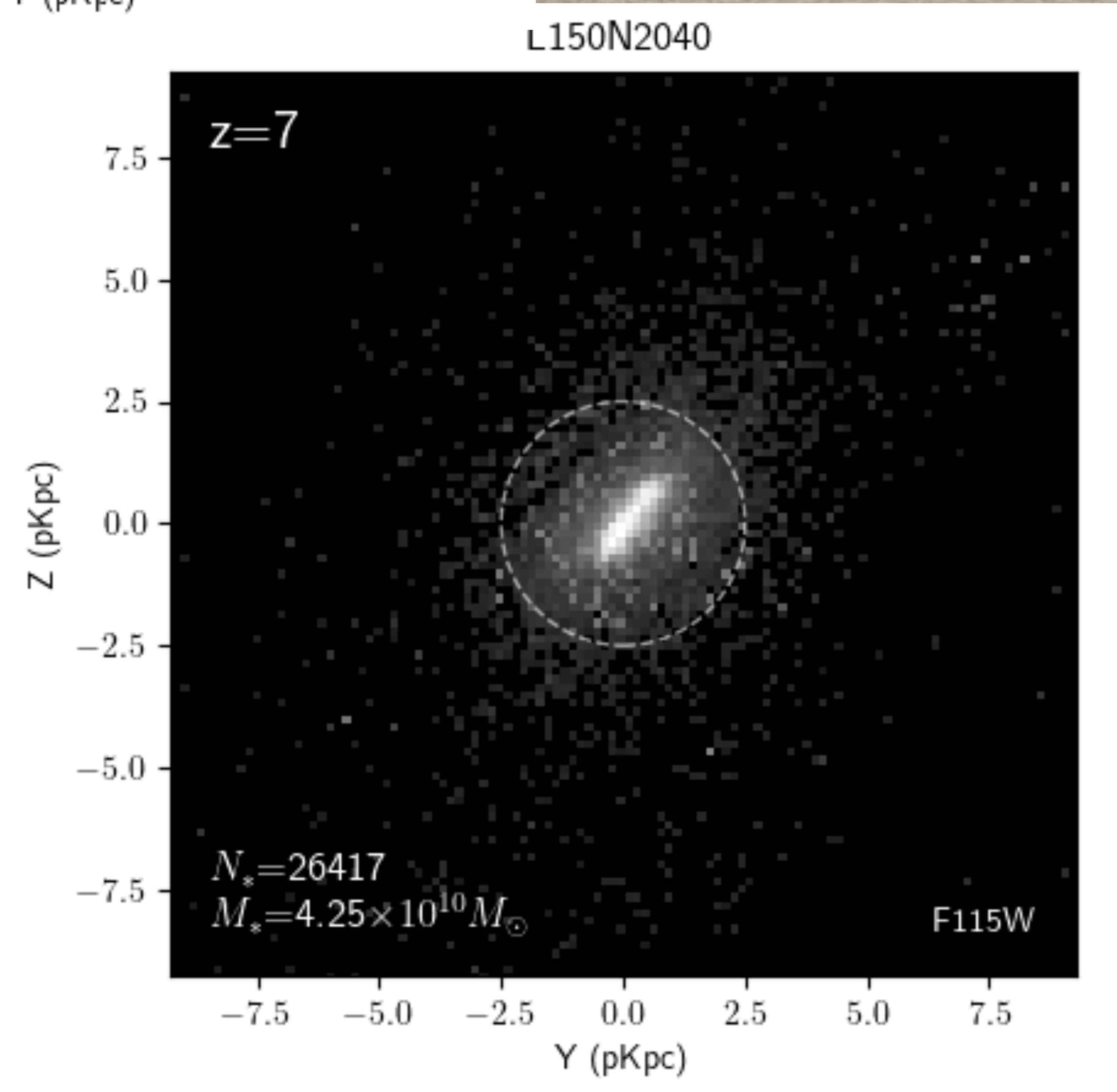

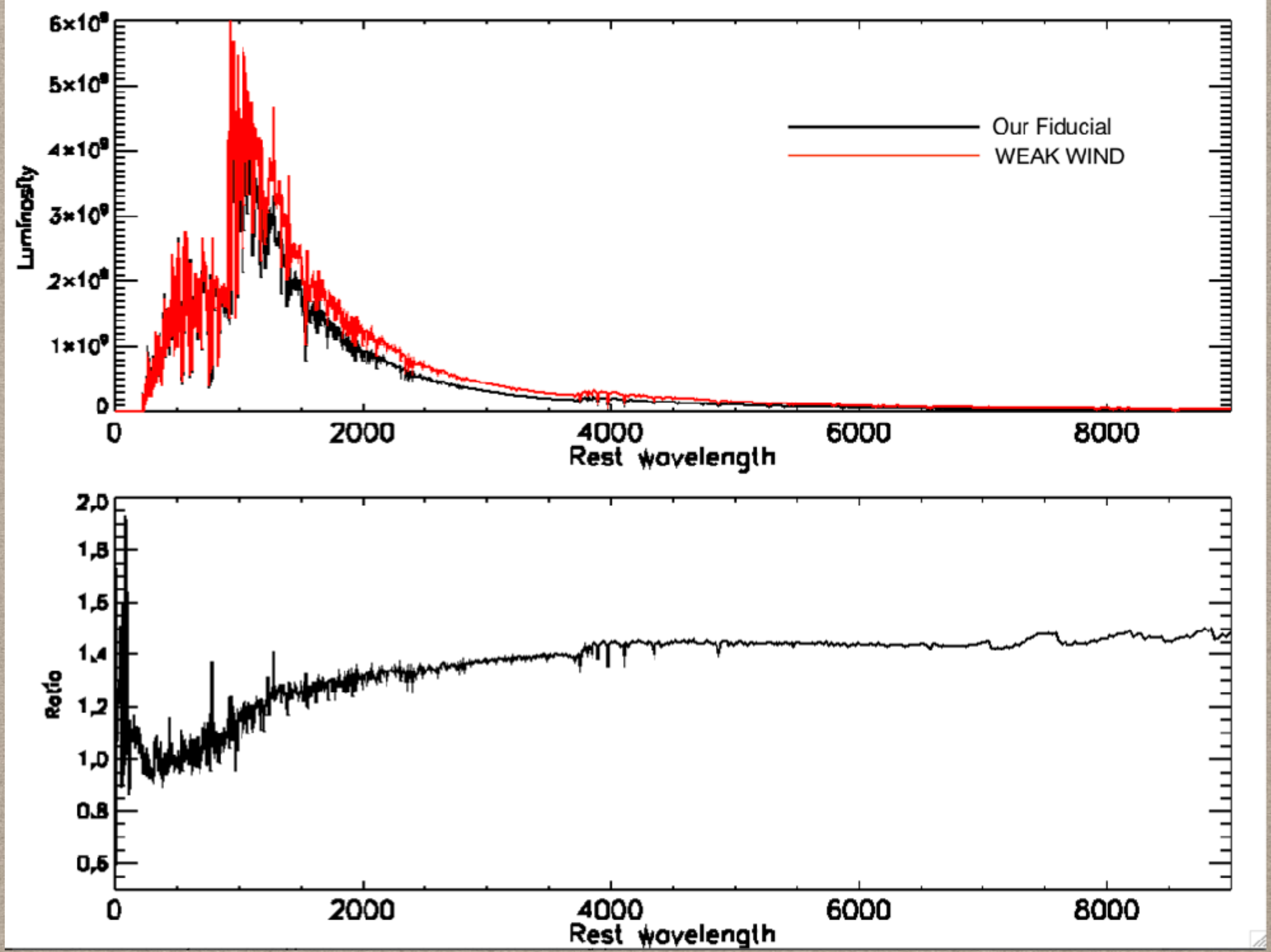

JWST: COMPOSITE SPECTRA OF HIGH-Z GALAXIES

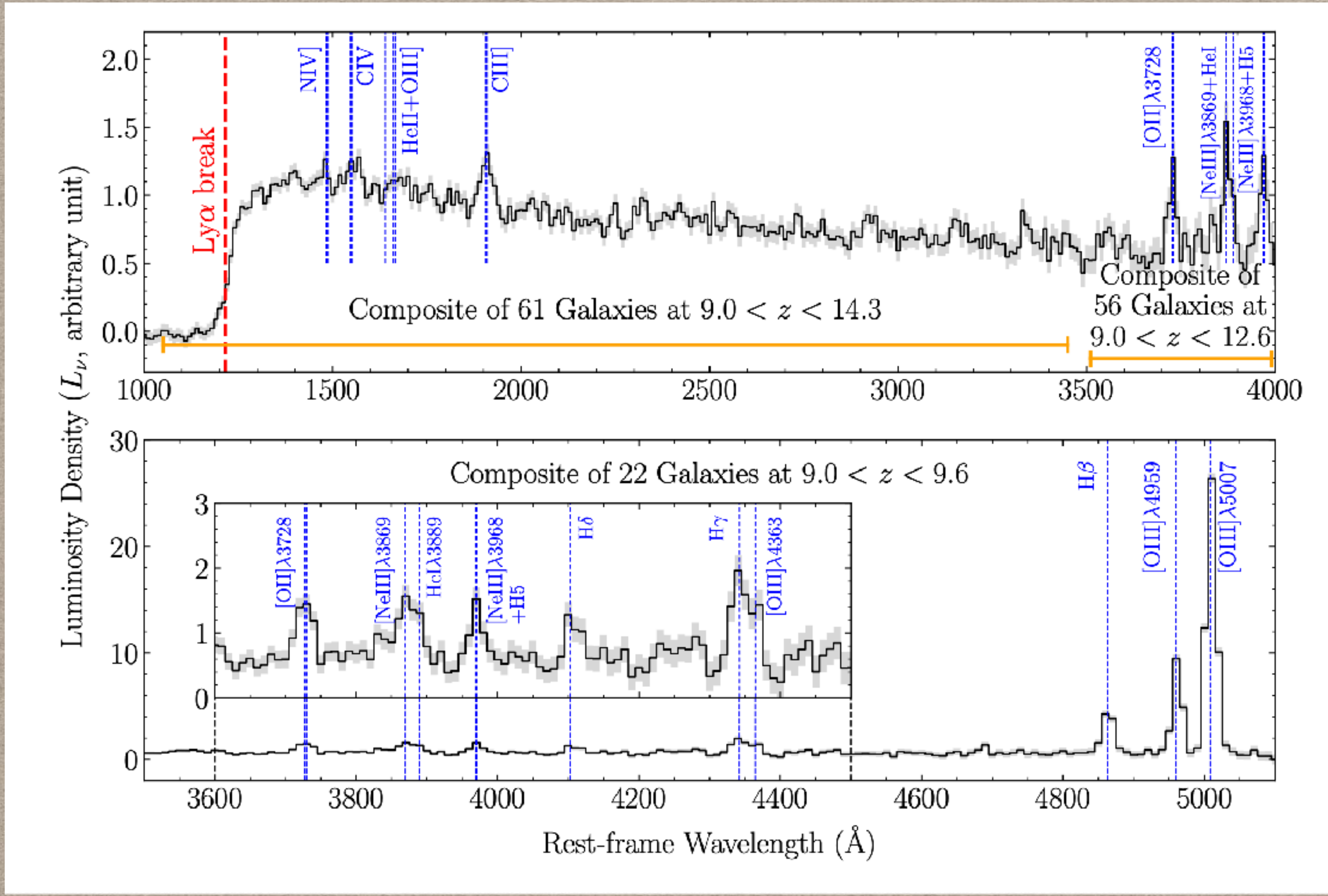

- C III], H-β, H-γ EWs are 2-3 time more at z>9 relative to those 6<z<9. Consistent with the expectations that the galaxy population is becoming more dominated recent burst of star-formation.
- UV slope β is found to be in the range -2.64 to -2.01. The mean is close to what is expected for stellar +nebular SED.
- CIV emission detected with10% showing strong CIV emission lines.
- Nature of ionising sources, metallicity, enrichment history and Pressure of the HII regions can be constrained.

Tang et al., arxiv:2507.082452

JWST: ABUNDANCE RATIO & CHEMICAL EVOLUTION

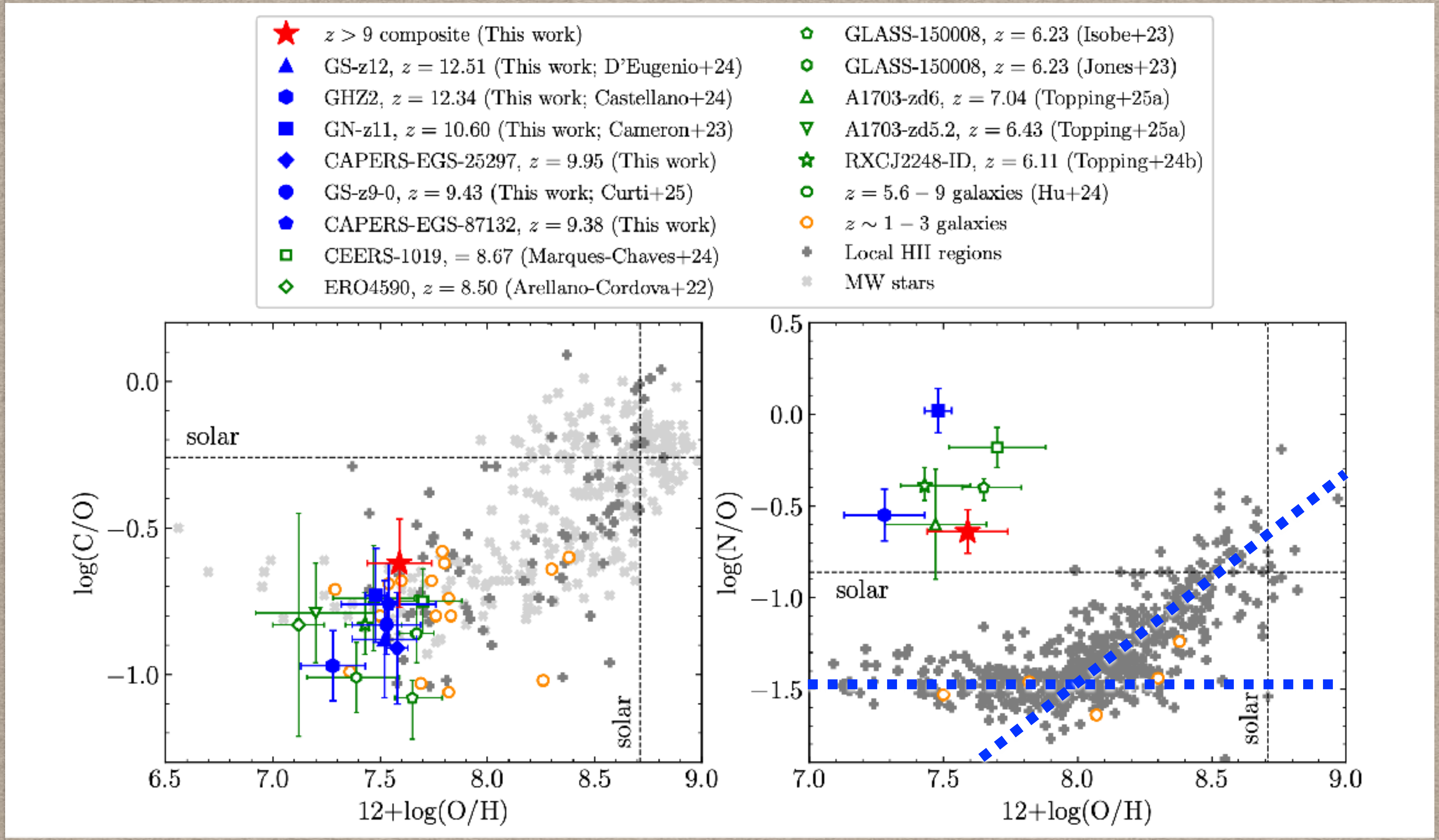

- $12 + \log(O/H) = 7.59^{+0.05}_{-0.05}$ That is 0.05 solar value. Moderately metal poor.
- [C/O] vs [O/H] follow the trend seen in low-z galaxies.
- Galaxies at z>9 seem to have nitrogen enhanced metallicity conditions.

Tang et al., arxiv:2507.082452

LITTLE RED DOTS

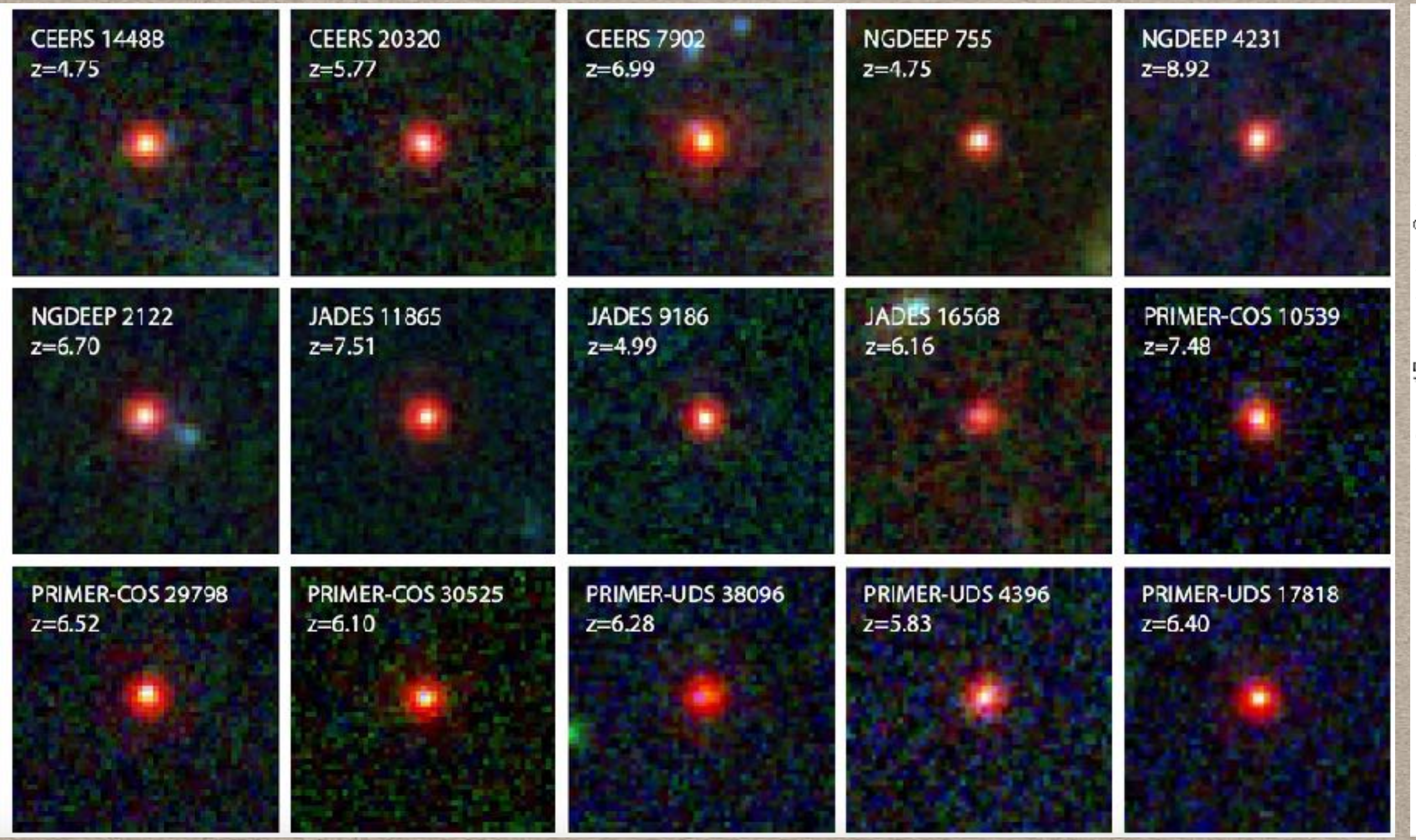

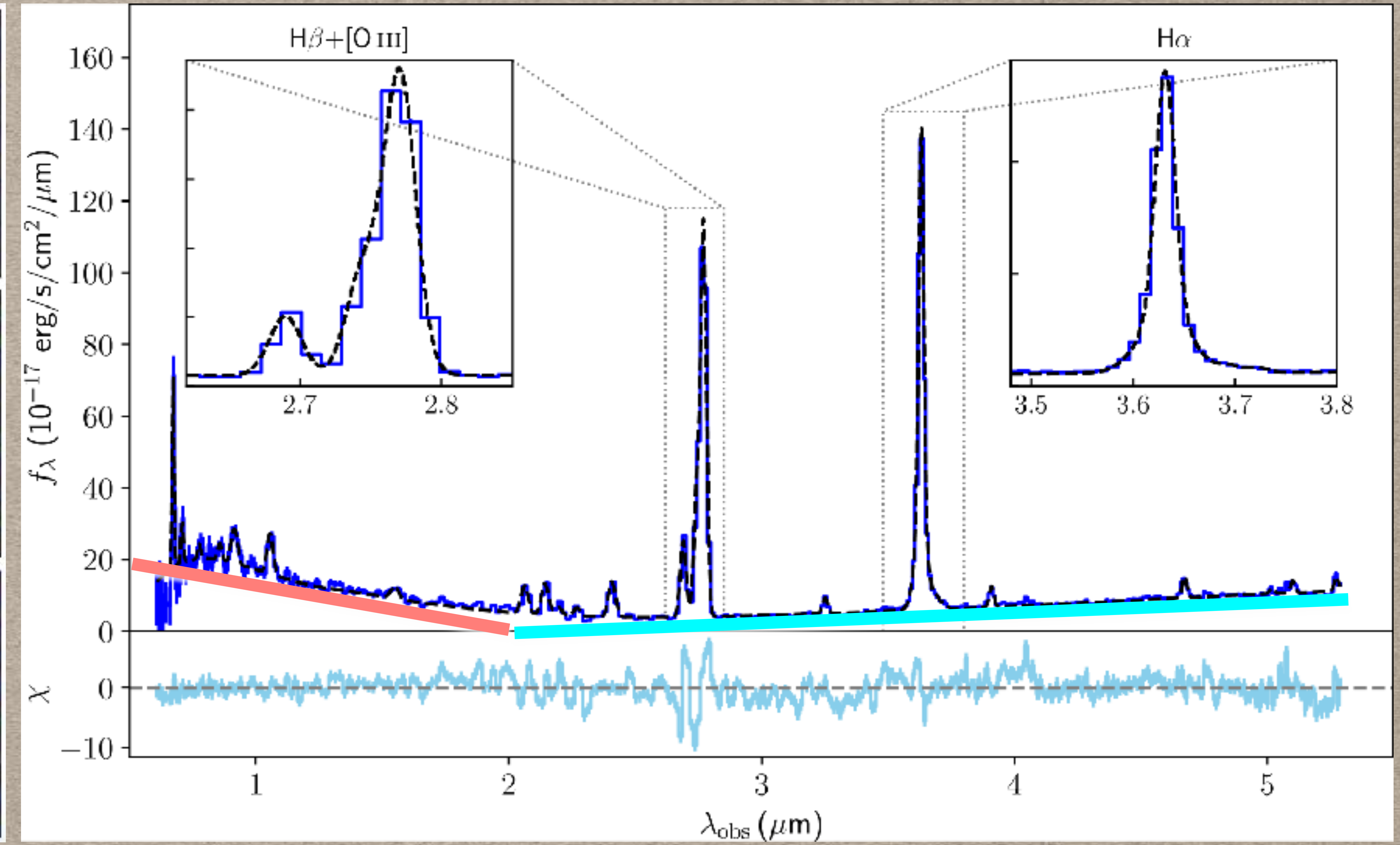

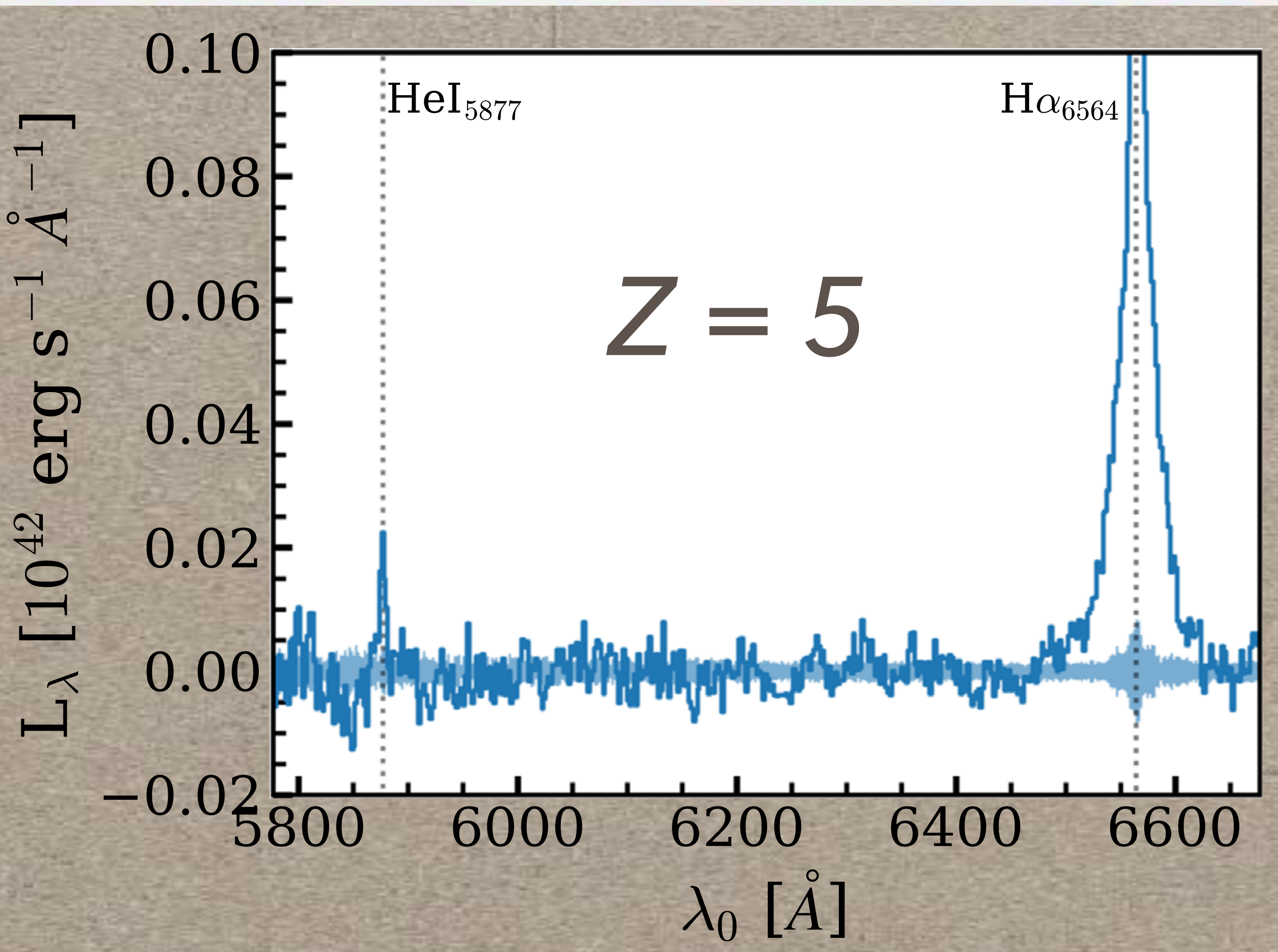

- Understanding the origin of LRDs is important for our understanding of SMBH in early universe. How to seed these BHs?
- Can one use the standard relationship between width of Hα line and M_{BH}. Is there any alternate way of making the line wider -How to get so much dust so early.
- Implications to X-ray background, reionization (or heating of the IGM) and GW bar?

LITTLE RED DOTS

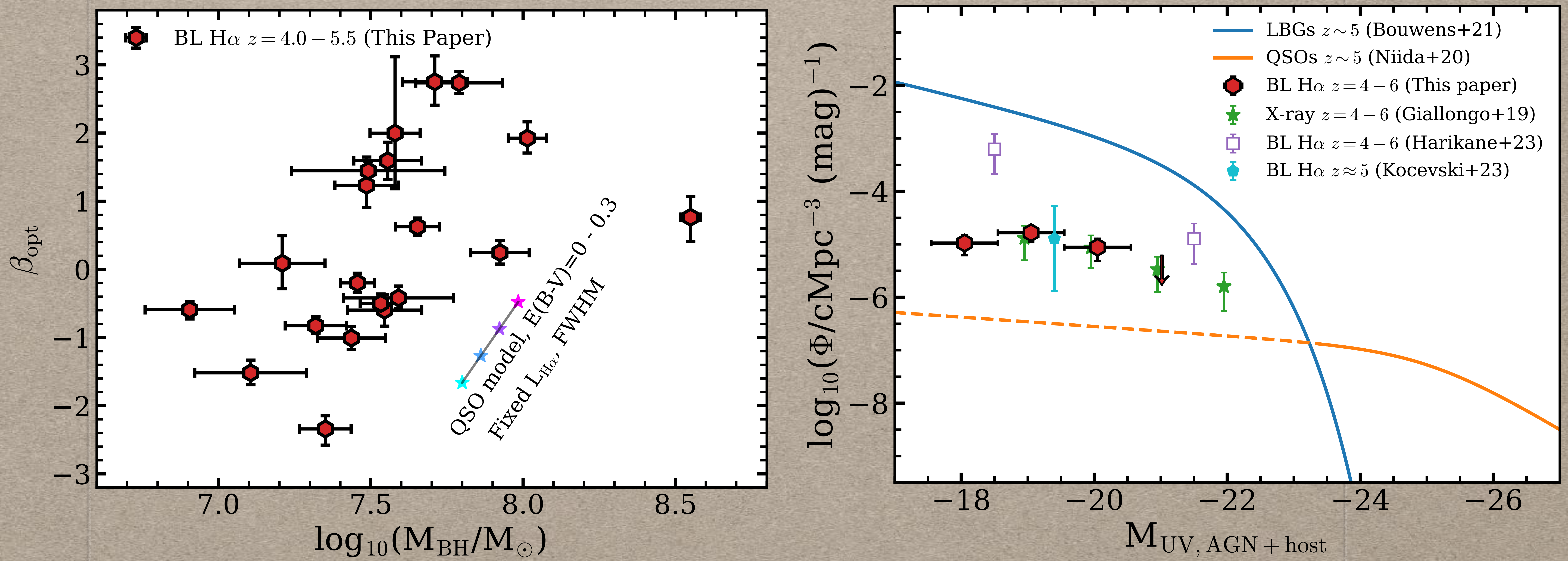

- Population of LRDs peak at high-z and fraction of galaxies hosting them seems to be high at z>6.

Ref: Matthew et al., 2024, ApJ, 963,129

WHAT ARE IN THE PIPELINE!

- Getting the BH number densities correctly - BH merger rates and GW signals
- LF in mm range, CII, CI and nebular line luminosities etc..
- Reionization models (as a post processing step).
- Running the simulations in patchy regions. (Nishi + Prakash)
- Dust and Lya radiative transport inside the galaxy (Soumak & Supriyo, TIFR)
- Radiative transport outside the galaxy and metal pollution as a function of feedback parameters (Prakash & Manish, IIT, Indore).
- Low redshift CGM, IGM etc.. (Two Master students at NISER, BBSR)

THANKS